



UNIVERSITÀ
DEGLI STUDI
FIRENZE

FLORE

Repository istituzionale dell'Università degli Studi di Firenze

Imidazo[1,2-a]pyrazin-8-amine core for the design of new adenosine receptor antagonists: Structural exploration to target the A3 and A2A

Questa è la Versione finale referata (Post print/Accepted manuscript) della seguente pubblicazione:

Original Citation:

Imidazo[1,2-a]pyrazin-8-amine core for the design of new adenosine receptor antagonists: Structural exploration to target the A3 and A2A subtypes / Daniela Poli, ; Matteo Falsini, ; Flavia Varano, ; Marco Betti, ; Katia Varani, ; Fabrizio Vincenzi, ; Anna Maria Pugliese, ; Felicita Pedata, ; Diego Dal Ben, ; Ajiroghene Thomas, ; Ilaria Palchetti, ; Francesca Bettazzi, ; Daniela Catarzi, ; Colotta, Vittoria. - In:

Availability:

The webpage <https://hdl.handle.net/2158/1057625> of the repository was last updated on 2021-03-29T10:06:59Z

Published version:

DOI: 10.1016/j.ejmech.2016.09.076

Terms of use:

Open Access

La pubblicazione è resa disponibile sotto le norme e i termini della licenza di deposito, secondo quanto stabilito dalla Policy per l'accesso aperto dell'Università degli Studi di Firenze (<https://www.sba.unifi.it/upload/policy-oa-2016-1.pdf>)

Publisher copyright claim:

La data sopra indicata si riferisce all'ultimo aggiornamento della scheda del Repository FloRe - The above-mentioned date refers to the last update of the record in the Institutional Repository FloRe

(Article begins on next page)

Imidazo[1,2-*a*]pyrazin-8-amine core for the design of new adenosine receptor antagonists: structural exploration to target the A₃ and A_{2A} subtypes.

Daniela Poli,^a Matteo Falsini,^a Flavia Varano,^a Marco Betti,^a Katia Varani,^b Fabrizio Vincenzi,^b Anna Maria Pugliese,^c Felicita Pedata,^c Diego Dal Ben,^d Ajiroghene Thomas,^d Ilaria Palchetti,^{e,f} Francesca Bettazzi,^e Daniela Catarzi,^{a*} Vittoria Colotta^a

^aDipartimento di Neuroscienze, Psicologia, Area del Farmaco e Salute del Bambino, Sez. Farmaceutica e Nutraceutica, Università degli Studi di Firenze, Via Ugo Schiff 6, 50019 Sesto Fiorentino (FI) Italy; ^bDipartimento di Scienze Mediche, Sez. Farmacologia, Università degli Studi di Ferrara, Via Fossato di Mortara, 17-19, 4412 Ferrara, Italy; ^cDipartimento di Neuroscienze, Psicologia, Area del Farmaco e Salute del Bambino, Sez. Farmacologia e Tossicologia, Università degli Studi di Firenze, Viale Pieraccini, 6, 50139 Firenze, Italy; ^dScuola di Scienze del Farmaco e dei Prodotti della Salute, Università degli Studi di Camerino, Via S. Agostino 1, 62032 Camerino (MC), Italy; ^eDipartimento di Chimica “Ugo Schiff”, Università degli Studi di Firenze, Via della Lastruccia 3-13, 50019 Sesto Fiorentino (FI) Italy; ^fIstituto di Biochimica delle Proteine-CNR, Via P.Castellino 111, 80131 Napoli, Italy.

Corresponding author: Tel.: +39-055-4573722; fax: +39-055-4573780; e-mail: daniela.catarzi@unifi.it

Abbreviations: AR, adenosine receptor; AB-MECA, N⁶-(4-Aminobenzyl)-N-methylcarboxamidoadenosine; NECA, 5’-(N-ethyl-carboxamido)adenosine; Cl-IB-MECA, 2-chloro-N⁶-(3-iodobenzyl)5’-(N-methylcarbamoil)adenosine; DPCPX, 8-cyclopentyl-1,3-dipropyl-xanthine; ZM-241385, 4-(2-[7-amino-2-(2-furyl)[1,2,4]-triazolo[2,3-*a*][1,3,5]triazin-5-ylamino]ethyl)phenol; CHO, Chinese hamster ovary; EL2, second extracellular loop; MOE, molecular operating environment; MOPAC, molecular orbital PACkage; TM, transmembrane; OGD, oxygen and glucose deprivation; AD, anoxic depolarization; fEPSP, field excitatory postsynaptic potential; d.c., direct current.

Abstract.

The imidazo[1,2-*a*]pyrazine ring system has been chosen as a new decorable core skeleton for the design of novel adenosine receptor (AR) antagonists targeting either the human (h) A₃ or the hA_{2A} receptor subtype. The N⁸-(hetero)arylcarboxyamido substituted compounds **4-14** and **21-30**, bearing a 6-phenyl moiety or not, respectively, show good hA₃ receptor affinity and selectivity versus the other ARs. In contrast, the 8-amino-6-(hetero)aryl substituted derivatives designed for targeting the hA_{2A} receptor subtype (compounds **31-38**) and also the 6-phenyl analogues **18-20** do not bind the hA_{2A} AR, or show hA₁ or balanced hA₁/hA_{2A} AR affinity in the micromolar range. Molecular docking of the new hA₃ antagonists was carried out to depict their hypothetical binding mode to our refined model of the hA₃ receptor. Some derivatives were evaluated for their fluorescent potentiality and showed some fluorescent emission properties. One of the most active hA₃ antagonists herein reported, i.e. the 2,6-diphenyl-8-(3-pyridoylamino)imidazo[1,2-*a*]pyrazine **29**, tested in a rat model of cerebral ischemia, delayed the occurrence of anoxic depolarization caused by oxygen and glucose deprivation in the hippocampus and allowed disrupted synaptic activity to recover.

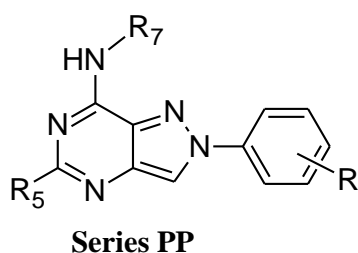
Keywords: G protein-coupled receptors, adenosine receptor antagonists, imidazopyrazines, bicyclic heteroaromatic systems, ligand-receptor modeling studies.

1. Introduction

Extracellular adenosine acts as an endogenous modulator in mammals through the activation of four cell surface adenosine receptors (ARs) classified as A₁, A_{2A}, A_{2B}, and A₃ [1]. Every AR subtype belongs to the G protein-coupled receptor (GPCR) family and mediates distinct physiological actions by coupling with different secondary messenger systems. Among the latter, adenylate cyclase (AC) is considered the principal effector system which can be either inhibited (A₁ and A₃) or stimulated (A_{2A} and A_{2B}), thus decreasing or increasing, respectively, cAMP production [1-3]. ARs, which are ubiquitously expressed in the human body, mediate a large number of physiological and pathophysiological processes. Thus, selective modulation of each receptor subtype could be utilized to therapeutic advantage [4]. In fact, there is ample evidence that ARs could be promising therapeutic targets for many pathological conditions.

In particular, the A₃AR has recently been found to be very interesting since it is associated with important neuroprotective effects, despite its low expression in the brain [5]. However, it has to be noted that the role of A₃AR in several neurological diseases is often controversial [6, 7]. Its inhibition by selective antagonists has been reported to be potentially neuroprotective after brain injury [8]. Thus, although to date a considerable number of selective A₃AR modulators have been discovered, much is still to be learned about the exact function of this receptor subtype in ischemia. A similar enigmatic role can be attributed also to the adenosine A_{2A} subtype which has recently emerged as an interesting target in ischemia as being involved in the modulation of brain damage after injury. However, the length of the time window in which the A_{2A} receptor plays a harmful or protective role after ischemic insult is still to be determined [9]. Thus, for both A₃ and A_{2A} receptors, it is intriguing to clarify whether and in which cases, selective agonist or antagonists could represent the best choice. In the light of the fact that no promising therapy is yet available for acute ischemic stroke, many scientists indicate adenosine as a target for possible therapeutic implementation.

Starting from the classical AR antagonist tricyclic core [4, 8, 10-12], bicyclic and monocyclic scaffolds have been evaluated in order to explore the structural requirements that could be important for the binding at the A₃ receptor subtype [13-18]. Evaluation of simplified core skeletons to obtain new AR antagonists have confirmed that, in some cases, structural simplification can represent a drug design strategy for maintaining or enhancing the biological activity of the original candidate [13, 14, 17]. Recently, we embarked on a research program to develop a new class of bicyclic compounds targeting the ARs, the 2-arylpyrazolo[4,3-*d*]pyrimidines (**PP**) [16, 19] (Figure 1), which show promise for the development of hA₃ AR antagonists. Structure activity relationship (SAR) studies on these compounds have led us to deduce some structural features that could be important for hA₃ receptor-ligand interaction and selectivity.



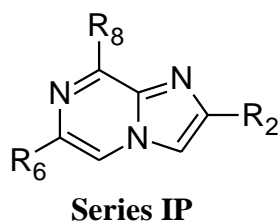
$R = H, 4\text{-OCH}_3, 4\text{-CH}_3$

$R_5 = \text{CH}_3, \text{C}_6\text{H}_5, \text{CH}_2\text{C}_6\text{H}_5$

$R_7 = H, \text{COAlk}, \text{COAr}, \text{COHetAr}$

Figure 1. Previously reported pyrazolo[4,3-*d*]pyrimidine derivatives (**PP**).

On this basis, in the present work, we studied a series of 2-arylimidazo[1,2-*a*]pyrazine-8-amine (**IP**, Figure 2) derivatives in order to obtain new potent and selective hA_3 AR antagonists and also to preliminarily evaluate the structural modifications to be performed on this series to target the hA_{2A} subtype.



Targeting the hA_3 AR

$R_2 = \text{C}_6\text{H}_5, 4\text{-CH}_3\text{OC}_6\text{H}_4, \text{furan-2-yl}$

$R_6 = H, \text{C}_6\text{H}_5$

$R_8 = \text{NH}_2, \text{NHCOAr}, \text{NHCOHetAr},$
 $\text{N}(\text{COAr})_2, \text{NHCONHC}_6\text{H}_5$

Targeting the hA_{2A} AR

$R_2 = \text{C}_6\text{H}_5, \text{furan-2-yl}$

$R_6 = \text{Aryl}, \text{furan-2-yl}$

$R_8 = \text{NH}_2$

Figure 2. Currently reported imidazo[1,2-*a*]pyrazine derivatives as AR antagonists.

Firstly, we investigated the A_3 pharmacophore by choosing R_2 , R_6 and R_8 substituents on the basis of the SAR studies performed on our previously described derivatives [14-16, 18] and on many other structurally correlated classes of AR antagonists [4, 20-22]. Thus, starting from the imidazo[1,2-*a*]pyrazine-8-amine core skeleton, both the suitable phenyl and 4-methoxyphenyl substituents were introduced at position 2, but also the less usual furan-2-yl moiety was evaluated for hA_3 affinity. At

the same time, the 8-amino group was transformed into the canonical N⁸-heteroaryl-carboxyamido- or N⁸-phenylureido-function. In the first set of compounds (**1-14**), position 6 was maintained unsubstituted (R₆=H). For comparison, in the second set of derivatives, a phenyl moiety (**18-30**) or a bromine atom (**15-17**) was introduced at R₆ to evaluate the importance of a lipophilic substituent at this position. In this part of our study, it emerged that the contemporary presence of a lipophilic substituent at position 6 (the phenyl moiety, i.e. compounds **18-20** but also the bromine atom in **15-17**), and of the primary 8-amino group leads to an increased affinity for the hA_{2A} and/or hA₁ ARs. These data encouraged us to start a preliminary investigation on 6-(hetero)aryl substituted compounds (Figure 2) whose R₆ substituents were chosen on the basis of literature data of similar bicyclic A_{2A} antagonists [19, 23-25].

It is important to underline that we have focused our attention on the imidazo[1,2-*a*]pyrazine-8-amine scaffold because the 2-phenyl-substituted compound **1**, although being totally inactive at all the AR subtypes, possesses some fluorescent emission property. Thus, it might have been a promising starting point for developing fluorescent AR antagonists. In particular, the imidazo[1,2-*a*]pyrazine scaffold closely resembles that of other bicyclic heteroaromatic ring systems with documented fluorescent properties [26, 27]. For our purpose, we decided to decorate the core skeleton to optimize its fluorescence emission and AR affinity at the same time. In this, we were hoping to be helped by the fact that some substituents in precise positions, i.e. the methoxy group, as well as being reported as profitable for A₃ affinity [14, 16], are so far improving fluorescence properties [27].

Thus, all the new derivatives (**1-38**) were tested to evaluate their affinities at hA₁, hA_{2A} and hA₃ ARs and their efficacy at hA_{2B} subtype. Considering the imidazo[1,2-*a*]pyrazine scaffold as a new structural motif for the design of AR antagonists, a few selected compounds (**1**, **5**, **21**, **22**, **29**) were also tested in cAMP functional assays to assess their hA₃ antagonistic activity. In addition, the measurement of some photophysical properties for some derivatives was performed.

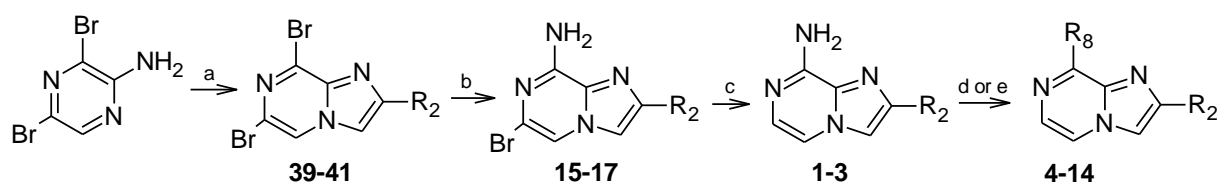
One of the most interesting compounds (**29**) in terms of hA₃ AR affinity and selectivity was also evaluated in an *in vitro* rat model of cerebral ischemia, since in previous studies [11, 12] structurally related compounds proved to be effective in preventing the failure of synaptic activity induced by oxygen and glucose deprivation (OGD) in the hippocampus.

Along with the pharmacological evaluation, molecular docking of this new class of hA₃ AR antagonists was carried out to depict their hypothetical binding mode to an hA₃ receptor model.

2. Chemistry

The imidazo[1,2-*a*]pyrazine derivatives **1-38** were synthesized as depicted in Schemes 1-3. The N⁸-substituted compounds **4-14** together with the corresponding 8-amino intermediates **1-3** were

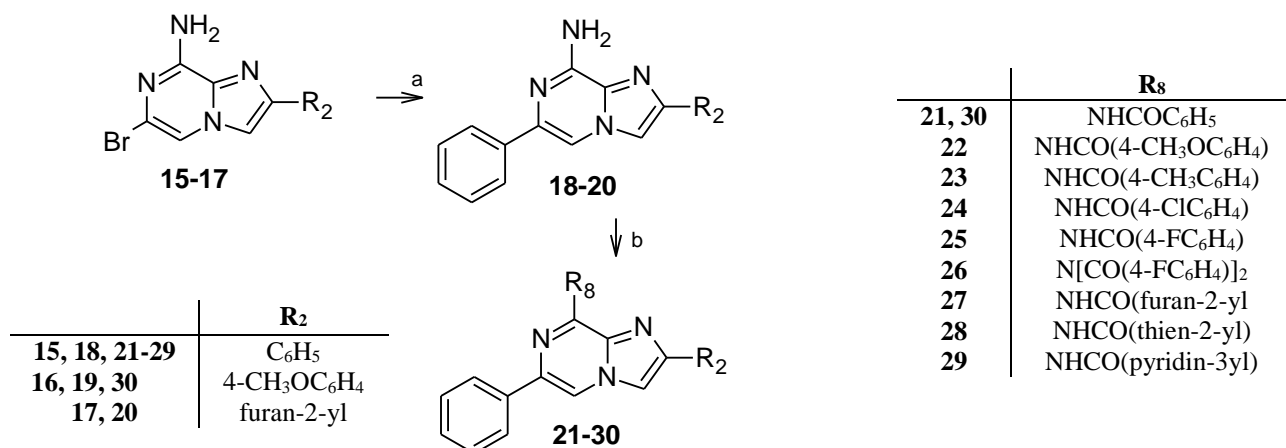
prepared according to the procedure described in Scheme 1. By reacting the 3,5-dibromo-2-aminopirazine [28] with the suitable α -bromoketone [29] in solvent-free conditions, the 6,8-dibromo-derivatives **39-41** [30] were obtained with high yields. Regiospecific displacement of the 8-bromo atom with ammonia in absolute ethanol at 120°C in an autoclave gave the 8-amino-derivatives **15-17**. Catalytic dehalogenation with Pd/C yielded compounds **1-3** which were acylated at the 8-amino-substituent for obtaining the corresponding amido-derivatives **4-13**. The reaction can be performed with the suitable aroyl chloride in tetrahydrofuran containing pyridine (compounds **4, 5**) or by using the necessary carboxylic acid in the presence of group activators (derivatives **6-13**). The 8-ureido derivative **14** was obtained by reacting the 8-amino-2-phenyl compound **1** with phenylisocyanate in dichloromethane at room temperature for a long reaction time.



	R₂		R₈		R₈
39, 15, 1, 4-11, 14	C ₆ H ₅	4, 12, 13	NHCOC ₆ H ₅	9	NHCOCH(C ₆ H ₅) ₂
40, 16, 2, 12	4-CH ₃ OC ₆ H ₄	5	N(COC ₆ H ₅) ₂	10	NHCO(furan-2-yl)
41, 17, 3, 13	furan-2-yl	6	NHCO(4-CH ₃ OC ₆ H ₄)	11	NHCO(pyridin-3-yl)
		7	NHCO(4-CH ₃ C ₆ H ₄)	14	NHCONHC ₆ H ₅
		8	NHCOCH ₂ C ₆ H ₅		

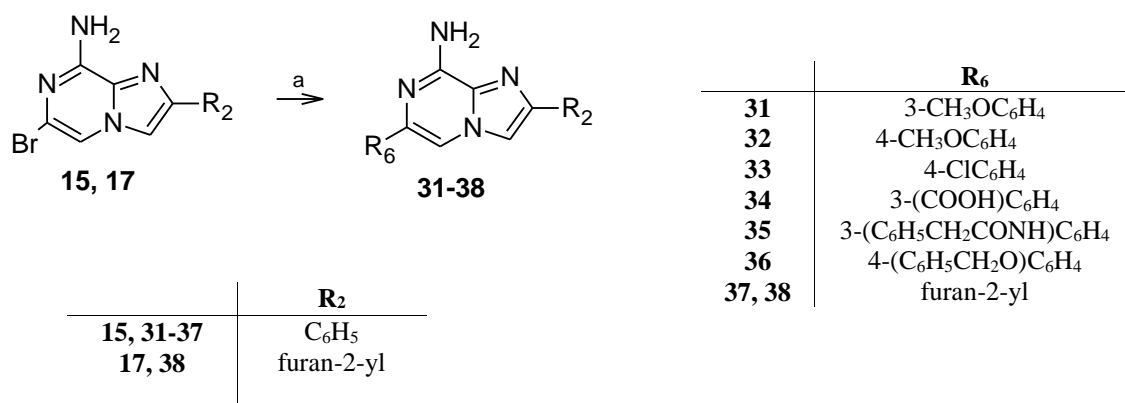
Scheme 1. Reagents and conditions: a) BrCH₂COR₂, 100°C; b) NH₃ (gas), absolute ethanol, 120°C, autoclave; c) H₂, Pd/C, ethanol; d) RCOCl, anhydrous tetrahydrofuran, pyridine, reflux, or RCOOH, N-(3-dimethylammino-propyl)-N'-ethylcarbodiimide·HCl, 1-hydroxybenzotriazole hydrate, anhydrous dimethylformamide, r.t.; e) PhNCO, anhydrous dichloromethane, r.t.

The 6-phenyl-8-amino derivatives **18-20** were obtained by reacting the 6-bromo-derivatives **15-17** with phenylboronic acid in 1,2-dimethoxyethane/water in the presence of tetrakis and sodium carbonate (Scheme 2). Then, the 8-amino group was reacted with the suitable aroyl chloride in anhydrous pyridine at reflux to yield the desired compounds **21-30**.



Scheme 2. Reagents and conditions: a) C₆H₅B(OH)₂, tetrakis, Na₂CO₃, 1,2-dimethoxyethane/water 3:1, 85°C; b) RCOCl, pyridine, reflux.

Scheme 3 depicts the synthesis of compounds **31-38** which bear different substituents at the R₆ position. These derivatives were obtained by reaction of **15**, **17** with the suitable boronic acid, all commercially available with the exception of the 3-(2-phenylacetamido)phenyl boronic acid **42**, that was obtained by acylation of the 3-aminophenylboronic acid with 2-phenylacetyl chloride in tetrahydrofuran containing trimethylamine (see experimental section).



Scheme 3. Reagents and conditions: a) Commercially available R₆B(OH)₂ or **42** (R₆ = 3-(C₆H₅CH₂CONH)C₆H₄), tetrakis, Na₂CO₃, dimethoxyethane/water 3:1, 85°C.

3. Pharmacology.

All the reported compounds **1-38**, were tested for their ability to displace specific [³H]DPCPX, [³H]ZM241385 and [¹²⁵I]AB-MECA binding from hA₁, hA_{2A} and hA₃ receptors, respectively. The potency of the compounds at the hA_{2B} subtype was investigated by measuring their inhibitory effect on 200 nM NECA-stimulated cAMP levels in Chinese hamster ovary (CHO) cells transfected with

the hA_{2B} receptor. The affinity (expressed as K_i) and potency (expressed as IC₅₀) values of the novel compounds are reported in Tables 1-2. Moreover, to evaluate the hA₃ AR antagonistic effect, compounds **4**, **5**, **21**, **22**, **29** were tested for their ability to counteract the 100 nM Cl-IB-MECA-mediated inhibition of cAMP production in CHO cells expressing hA₃ AR. On the same set of compounds, rat (r) A₃ AR affinity values were evaluated using [¹²⁵I]AB-MECA in membranes from CHO cells transfected with rA₃ ARs (Table 3). Compound **29** was selected to evaluate its effect in an *in vitro* rat model of cerebral ischemia obtained by oxygen and glucose deprivation (OGD).

4. Fluorescence evaluation.

The fluorescent properties of some imidazopyrazine derivatives are listed in Table 4. Excitation and emission spectra were generally obtained from solutions of the compounds in CHCl₃. To probe the environment affecting the sensitivity of the fluorescent compound, the quantum yield (Φ) values of the selected derivatives **1**, **5**, **6** and **13** were determined also in a polar solvent, i.e. EtOH. Lower Φ values are expected in polar solution compared to nonpolar solvents. In fact, the highest Φ values were those recorded in CHCl₃. The fluorescence quantum yield was calculated by using the fluorescent 2-aminopyridine in 0.1 M H₂SO₄ solution (Φ = 0.6, excitation wavelength (λ_{ex}) = 285nm) as reference compound.

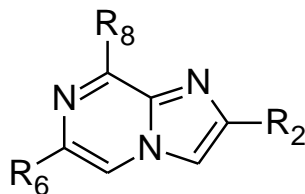
5. Results and discussion.

5.1. Structure-affinity relationship studies and fluorescence properties.

As shown in Tables 1 and 2, while most of the synthesized compounds targeting the hA₃ AR (derivatives **4-14** and **21-30**) have affinity in the nanomolar range and selectivity for this subtype, only a few derivatives designed as A_{2A} AR antagonists (compounds **31-38**) together with the 6-phenyl substituted analogues **18-20** have A₁ or balanced A₁/A_{2A} AR affinity in the micromolar range. These data suggest that the imidazo[1,2-*a*]pyrazine ring system can be considered as a new scaffold for the development of potent and selective hA₃ AR antagonists. Starting from the 2-phenylimidazo[1,2-*a*]pyrazine-8-amine **1** (Table 1), other compounds bearing different substituents on the 8-amino group were synthesized (**4-14**, **21-30**). Introduction of the benzoyl group, once (compound **4**) or twice (derivative **5**) on the 8-amino function, leads to potent and selective hA₃ AR antagonists. In contrast, the presence at position 8 of different N-(hetero)arylcarboxyamido groups does not have a profitable effect, with the exception of compounds **6**, **8** and **9** that show hA₃ affinity in the micromolar range. Nor did the insertion of the phenylureido substituent at position 8 have a positive effect on the hA₃ binding leading to the inactive compound **14**. The same applies to the 2-(4-methoxyphenyl) substituent that does not lead to significant modification of hA₃ AR affinity (compare **2** and **12** with

1 and **4**, respectively) as described for previously reported derivatives [16]. In contrast, the presence of the more polar 2-(furan-2-yl) moiety in the 8-benzoylamino derivative **13** produces a total loss of hA₃ binding affinity compared to **4**.

Table 1. Binding affinity (K_i) at hA₁, hA_{2A} and hA₃ ARs and potencies (IC₅₀) at hA_{2B}.



	R ₂	R ₆	R ₈	Binding experiments ^a K _i (nM) or I%			cAMP assay I%
				hA ₁ ^b	hA _{2A} ^c	hA ₃ ^d	hA _{2B} ^e
1	C ₆ H ₅	H	NH ₂	30%	13%	12%	30%
2	4-CH ₃ O-C ₆ H ₄	H	NH ₂	1%	1%	1%	1%
3	2-furanyl	H	NH ₂	21%	12%	5%	1%
4	C ₆ H ₅	H	NHCOC ₆ H ₅	18%	1%	52 ± 5	2%
5	C ₆ H ₅	H	N(COC ₆ H ₅) ₂	4%	5%	64 ± 6	3%
6	C ₆ H ₅	H	NHCO(4-CH ₃ O-C ₆ H ₄)	1%	3%	162 ± 14	1%
7	C ₆ H ₅	H	NHCO(4-CH ₃ -C ₆ H ₄)	26%	21%	45%	10%
8	C ₆ H ₅	H	NHCOCH ₂ C ₆ H ₅	46%	37%	524 ± 47	15%
9	C ₆ H ₅	H	NHCOCH(C ₆ H ₅) ₂	32%	1%	245 ± 22	25%
10	C ₆ H ₅	H	NHCO(2-furanyl)	25%	34%	40%	19%
11	C ₆ H ₅	H	NHCO(3-pyridyl)	24%	13%	42%	22%
12	4-CH ₃ O-C ₆ H ₄	H	NHCOC ₆ H ₅	1%	1%	121 ± 11	1%
13	2-furanyl	H	NHCOC ₆ H ₅	7%	1%	22%	1%
14	C ₆ H ₅	H	NHCONHC ₆ H ₅	1%	1%	6%	1%
15	C ₆ H ₅	Br	NH ₂	420 ± 40	18%	14%	40%
16	4-CH ₃ O-C ₆ H ₄	Br	NH ₂	29%	11%	24%	27%
17	2-furanyl	Br	NH ₂	210 ± 18	265 ± 21	28%	29%
18	C ₆ H ₅	C ₆ H ₅	NH ₂	180 ± 15	310 ± 26	23%	36%
19	4-CH ₃ O-C ₆ H ₄	C ₆ H ₅	NH ₂	524 ± 47	1%	27%	1%

20	2-furanyl	C ₆ H ₅	NH ₂	143 ± 11	520 ± 46	21%	10%
21	C ₆ H ₅	C ₆ H ₅	NHCOC ₆ H ₅	1%	1%	82 ± 7	1%
22	C ₆ H ₅	C ₆ H ₅	NHCO(4-CH ₃ O-C ₆ H ₄)	6%	8%	25 ± 3	1%
23	C ₆ H ₅	C ₆ H ₅	NHCO(4-CH ₃ -C ₆ H ₄)	1%	1%	223 ± 21	3%
24	C ₆ H ₅	C ₆ H ₅	NHCO(4-Cl-C ₆ H ₄)	1%	1%	156 ± 12	1%
25	C ₆ H ₅	C ₆ H ₅	NHCO(4-F-C ₆ H ₄)	1%	1%	38 ± 4	2%
26	C ₆ H ₅	C ₆ H ₅	N(CO4-F-C ₆ H ₄) ₂	1%	1%	31%	3%
27	C ₆ H ₅	C ₆ H ₅	NHCO(2-furanyl)	10%	1%	67 ± 7	2%
28	C ₆ H ₅	C ₆ H ₅	NHCO(2-thienyl)	5%	1%	185 ± 16	4%
29	C ₆ H ₅	C ₆ H ₅	NHCO(3-pyridyl)	11%	1%	54 ± 6	3%
30	4-CH ₃ O-C ₆ H ₄	C ₆ H ₅	NHCOC ₆ H ₅	3%	1%	312 ± 32	1%

^a K_i values are means ± SEM of four separate assays each performed in duplicate. Percentage of inhibition (I%) is determined at 1 μM concentration of the tested compounds.

^b Displacement of specific [³H]DPCPX competition binding to hA₁CHO cells.

^c Displacement of specific [³H]ZM241385 competition binding to hA_{2A}CHO cells.

^d Displacement of specific [¹²⁵I]AB-MECA competition binding to hA₃CHO cells.

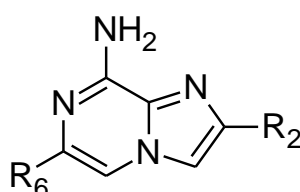
^e Percentage of inhibition on cAMP experiments in hA_{2B}CHO cells, stimulated by 200 nM NECA, at 1 μM concentration of the examined compounds.

The binding affinities of the 8-bromo substituted compounds **15-17**, selected among the synthetic intermediates, were evaluated. The presence of the 8-bromo atom enhanced the hA₁ (compound **15** vs **1**) or hA₁ and hA_{2A} affinity (compare **17** to **3**). While the 2-(furan-2-yl) compound **17** shows balanced hA₁/A_{2A} binding affinities, the corresponding 2-phenyl derivatives **15** preferentially binds the hA₁ AR. In contrast, the presence of the 8-bromo atom has no profitable effect on the binding of the 2-(4-methoxyphenyl) substituted compound **16** when compared to **2**.

When a phenyl group was introduced at position 6 of derivative **1-3**, the corresponding compounds **18-20** were obtained, all three showing enhanced binding affinity for the hA₁ AR. The same applies for the A_{2A} AR with the exception of compound **19** that does not bind this subtype. Acylation of the 8-amino group produced a new set of hA₃ AR antagonists (compounds **21-30**). Compound **22**, the 8-(4-methoxybenzoyl)amino substituted, emerges as the most active among the 6-phenyl-imidazopyrazines herein reported but closely followed by the 8-(4-fluorobenzoyl)amino derivative **25** and the 8-(3-pyridinoyl)amino compound **29**. By comparison with the unsubstituted analogues at R₆, it emerges that the 6-phenyl group has a profitable effect on hA₃ binding affinity of these derivatives. In fact, while the affinity of the 8-benzoylamino compound **21** is comparable to that of **4**, for the other substituted compounds the binding is ameliorated (compare **22** and **23** to **6** and **7**, respectively) or highly increased (compare **27** and **29** to **10** and **11**, respectively).

In Table 2, the pharmacological data of the imidazo[1,2-*a*]pyrazine-8-amine derivatives designed for targeting the hA_{2A} subtype are reported. The idea to start this preliminary structural investigation ensued from considerations that the contemporary presence of the primary 8-amino group and of a substituent at 6 position, either the phenyl or the 2-furanyl moiety (compounds **18-20**) leads to increased hA_{2A} and/or hA₁ AR affinities.

Table 2. Binding affinity (K_i) at hA₁, hA_{2A} and hA₃ ARs and potencies (IC₅₀) at hA_{2B}.



	R ₂	R ₆	Binding experiments ^a K _i (nM) or I%			cAMP assay I%
			hA ₁ ^b	hA _{2A} ^c	hA ₃ ^d	hA _{2B} ^e
31	C ₆ H ₅	3-CH ₃ O-C ₆ H ₄	37%	24%	21%	30%
32	C ₆ H ₅	4-CH ₃ O-C ₆ H ₄	20%	23%	23%	16%
33	C ₆ H ₅	4-Cl-C ₆ H ₄	3%	1%	1%	2%
34	C ₆ H ₅	3-COOH-C ₆ H ₄	7%	9%	1%	3%
35	C ₆ H ₅	3-(NHCOCH ₂ C ₆ H ₅)C ₆ H ₄	37%	33%	8%	7%
36	C ₆ H ₅	4-(OCH ₂ C ₆ H ₅)C ₆ H ₄	10%	1%	1%	4%
37	C ₆ H ₅	2-furanyl	28%	38%	20%	13%
38	2-furanyl	2-furanyl	316 ± 28	854 ± 82	38%	30%

^a K_i values are means ± SEM of four separate assays each performed in duplicate. Percentage of inhibition (I%) is determined at 1 μM concentration of the tested compounds.

^b Displacement of specific [³H]DPCPX competition binding to hA₁CHO cells.

^c Displacement of specific [³H]ZM241385 competition binding to hA_{2A}CHO cells.

^d Displacement of specific [¹²⁵I]AB-MECA competition binding to hA₃CHO cells.

^e Percentage of inhibition on cAMP experiments in hA_{2B}CHO cells, stimulated by 200 nM NECA, at 1 μM concentration of the examined compounds.

Taking the 2,6-diphenylimidazo[1,2-*a*]pyrazine-8-amine derivative **18** as lead compound, and on the basis of literature data [25, 31], a few different aryl substituents and also the 2-furanyl moiety were introduced at position 6 (compounds **31-36** and **37-38**, respectively). All the performed modifications lead to a decrease in hA_{2A} binding affinity with respect to **18**. The results obtained modifying the R₆ substituent are not encouraging since the compounds binding the hA_{2A} receptor (**18**, **20** and **38**) also have affinity for the hA₁ subtype. Even the introduction of the furan-2-yl moiety at both positions

does not exert the expected positive effect on A_{2A} affinity, as suggested by SAR studies on structurally related A_{2A} antagonists [32]. In fact, compounds **20** and **38**, bearing the 2-furan-2-yl moiety at R₂ and at both positions 2 and 6, respectively, have A_{2A} affinities in the micromolar range as the 2-phenyl analogue **18**. The results obtained up to now on these R₆ substituted derivatives are, in our opinion, not intriguing enough to encourage further investigation in this direction.

The effect of compounds **4**, **5**, **21**, **22** and **29** on the CI-IB-MECA-inhibited cAMP accumulation in hA₃ CHO cells was also determined. In accordance with their hA₃ affinity, all the selected pyrazoloquinoline derivatives proved to be potent in this test, showing antagonistic behavior (Table 3).

Table 3. Antagonistic potencies at hA₃ and binding affinity at rA₃ AR of some selected derivatives.

	cAMP assays hA ₃ CHO cells IC ₅₀ (nM) ^a	[¹²⁵ I]ABMECA binding rat A ₃ CHO cells I% at 1 μM ^b
4	163 ± 12	2%
5	187 ± 15	1%
21	235 ± 19	2%
22	73 ± 6	1%
29	172 ± 13	2%

^a IC₅₀ values are expressed as means ± SEM of four independent cAMP experiments, performed in triplicate, in hA₃ CHO cells in the presence of 100 nM CI-IB-MECA. ^b Percentage of inhibition (I%) of specific binding to rA₃ CHO cells.

Since compound **29** was tested in an *in vitro* rat model of cerebral ischemia, its binding affinity for rA₃ AR was measured together with those of other selected compounds (**4**, **5**, **21** and **22**) (Table 3).

The data obtained indicate that all the tested compounds are devoid of any binding activity at the rA₃ receptor although being highly potent at the human one.

Considering the fluorescence properties of some selected imidazopyrazine derivatives determined in CHCl₃ solution (Table 4), we can observe that the structural modification carried out at R₂, R₆ and R₈ position on the imidazopyrazine core has little or no influence on either λ_{ex} or emission wavelengths (λ_{em}). Most of the compounds showed λ_{ex} in the middle UV region. The quantum yield (Φ) was calculated to probe the potentiality of these compounds in relation to their fluorescent properties. The generally low Φ values disappointed our expectations. In addition to this behavior, all the derivatives considered in this study have a maximal λ_{em} in the UV range, and this finding alone impeded their potentiality as fluorescent probes in biological assays.

Table 4. Fluorescence properties of some imidazopyrazine derivatives^a.

	λ_{ex} (nm)	λ_{em} (nm)	Φ		λ_{ex} (nm)	λ_{em} (nm)	Φ
1	261 (260)*	367 (364)*	0.303 (0.007)*	19	285	387	0.128
2	267	358	0.189	20	286	400	0.112
4	240	n.d.	n.d.	21	320	n.d.	n.d.
5	326 (250)*	389 (389)*	0.047 (0.006)*	22	287	389	n.d.
6	258 (255)*	380 (380)*	n.d. (0.004)*	27	281	400	n.d.
9	257	380	0.095	29	280	n.d.	n.d.
10	257	n.d.	n.d.	30	249	400	n.d.
11	270	n.d.	n.d.	37	280	400	0.177
12	264 (261)*	394 (395)*	n.d. (0.026)*	38	294	390	0.179
13	267	387	0.024				

^aExcitation and emission spectra were recorded by dissolving compounds in CHCl_3 or, otherwise stated,* in EtOH. Fluorescence quantum yield values (Φ) were calculated by using 2-aminopyridine dissolved in H_2SO_4 0.1 M ($\Phi = 0.6$, $\lambda_{\text{ex}} = 285\text{nm}$) as standard fluorescent compound; n.d. = not detectable.

Compound **1**, that represents one of the simplest structures among the tested compounds, showed the highest Φ value herein reported (0.303). It has to be noted that, similar to compound **1**, all the other derivatives bearing a free amino group at position 8 (compounds **2**, **19**, **20**, **37** and **38**) are endowed with Φ values ranging from 0.1 to 0.2. These data confirm that electron-donating substituents such as an amino group have a beneficial effect on fluorescence. The available data do not allow us to speculate on the effect of the methoxy electron-donating group on fluorescent properties of compounds [27].

5.2. Molecular modeling studies

To define the structural features at the basis of the different binding affinities of the new derivatives, a molecular docking analysis was performed on a homology model of hA_3AR developed by using the X-ray structure of the inverse agonist-bound $\text{hA}_{2\text{A}}\text{AR}$ as template (pdb code: 3EML; 2.6-Å resolution [33]). The $\text{A}_{2\text{A}}\text{AR}$ crystal structure improves the accuracy of AR homology models, due to the high residue conservation in the primary sequences of the AR subtypes, which share a sequence identity of ~57% within the transmembrane (TM) domains [34]. The residues located within the seven TM

domains in the upper part of ARs, corresponding to the ligand binding site, are conserved with an average identity of 71% [35]. Furthermore, the above cited A_{2A}AR crystal structure has been solved in complex with high affinity inverse agonist (ZM241385), and hence presents a cavity suitable as a binding site for docking analysis. The obtained hA₃AR homology model was checked by using the Protein Geometry Monitor application within Molecular Operating Environment (MOE) [36], which provides a variety of stereochemical measurements for inspection of the structural quality in a given protein, such as backbone bond lengths, angles and dihedrals, Ramachandran ϕ - ψ dihedral plots, and sidechain rotamer and nonbonded contact quality.

A preliminary docking analysis was performed by manually docking the high affinity antagonist MRS 1220 (K_i hA₃AR = 0.65 nM [37]) structure within the hA₃AR model binding site. The obtained hA₃AR-MRS 1220 complex was then subjected to energy minimization refinement and to Monte Carlo analysis to explore the favorable binding conformations. The input structure consisted of the ligand and a shell of receptor amino acids within 6 Å distance from the ligand. A second external shell of all the residues within a distance of 8 Å from the first shell was kept fixed. During the Monte Carlo conformational searching (10,000 steps), the input structure was modified by random changes in torsion angles (for all input structure residues), and molecular position (for the ligand). Hence, the ligand was left free to be continuously re-oriented and re-positioned within the binding site and the conformation of both ligand and internal shell residues could be explored and reciprocally relaxed. This stage allowed us to provide an A₃AR binding site conformation able to accommodate the analyzed antagonists. The best receptor-MRS 1220 complex was subjected to energy minimization. Once the MRS 1220 compound was removed, the hA₃AR model was then used as target for the docking analysis of synthesized derivatives. All ligand structures were optimized using RHF/AM1 semi-empirical calculations and the software package Molecular Orbital Package (MOPAC) implemented in MOE was utilized for these calculations [38]. The compounds were then docked into the binding site of the hA₃AR model by using the MOE Dock tool. Top-score docking poses of each compound were subjected to energy minimization and then rescored using three available methods implemented in MOE: the *London dG* scoring function that estimates the free energy of binding of the ligand from a given pose; the *Affinity dG* scoring tool that estimates the enthalpic contribution to the free energy of binding; the *dock-pK_i* predictor that uses the MOE *scoring.svl* script to estimate a pK_i value for each ligand, which is described by the H-bonds, transition metal interactions, and hydrophobic interactions energy. For each compound, the top-score docking poses, according to at least two out of three scoring functions, were selected for final ligand-target interaction analysis. Considering the binding mode of the imidazo[1,2-*a*]pyrazine derivatives in the hA₃AR, docking results present several possible orientations and conformations for the analyzed compounds, with a

conformation family energetically favored and statistically more represented compared to the others. It has to be noted that, in general, the two main series of compounds reported in Table 1, i.e. the 6-unsubstituted compounds **1-14** and those bearing the phenyl substituent at R₆ (derivatives **18-30**), have a similar binding mode. This binding mode shows the bicyclic scaffold vertically oriented with the imidazole ring almost externally located and the pyrazine ring positioned more in depth in the pocket. However, due to the presence or not of the 6-substituent, a few important differences have been evidenced justifying the discrepancy in binding results between the two series. In fact, since the 6-phenyl ring seems to act as an anchor point for the binding mode, the lack of this same substituent makes derivatives more able to move within the pocket.

For the 6-phenyl-substituted derivatives, the position of the bicyclic scaffold is stabilized by hydrophobic interactions with the second extracellular loop (EL2) (Phe168) and TM7 (Leu264 and Ile268 residues (Figure 3). The nitrogen atom at 1-position and the 8-NH group form a double H-bond interaction with the amide group of Asn250 (TM6) side chain, hence providing further anchor points to the scaffold for interaction with the receptor. This binding mode makes the 2-aromatic ring to be located at the entrance of the binding site in a region presenting some hydrophobic profile due to the presence of residues like Val169 (EL2) and Ile253 (TM6). Introduction of a methoxy group in *para*-position of the 2-phenyl ring leads to reduced affinity with respect to the unsubstituted analogue (**21**, K_i = 82 nM vs **30**, K_i = 312 nM), probably due to the exposure of this hydrophobic group to the solvent which possibly affects complex stability. Analogous behavior can be observed for the 6-unsubstituted derivatives (**4**, K_i = 52 nM vs **12**, K_i = 121 nM). The aromatic ring at R₆ is located in proximity of TM2 (Ala69 and Val72), TM3 (Leu90), EL2 (Phe168), and TM7 (Ile268) residues, in a small sub-pocket presenting a hydrophobic profile. Together with the 8-substituent, this group acts as a constraint, making the ligand orientation strongly anchored within the pocket. As previously observed, the binding mode of the 6-unsubstituted derivatives is very similar to the above described 6-phenyl analogs, with the 2-aromatic ring being located at the entrance of the binding site in a region presenting some hydrophobic profile due to the presence of residues like Val169 (EL2) and Ile253 (TM6). The 6-unsubstituted compounds move quite freely within the A₃ binding pocket, partially losing the reinforcing H-bond interaction with Asn250.

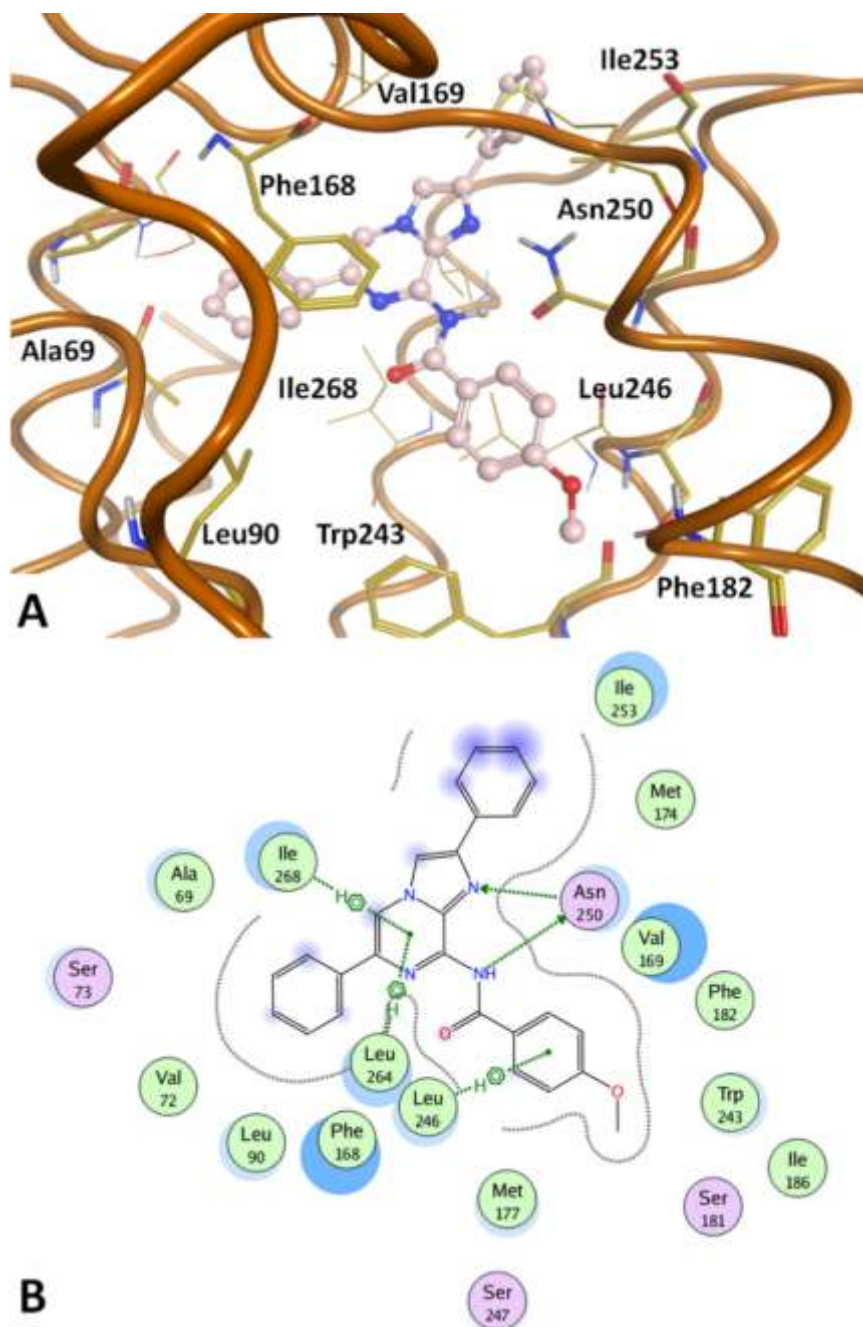


Figure 3. Docking conformations of the 2,6,8-substituted imidazopyrazine derivatives. **(A)** The binding mode of compound **22** at 3EML-based hA₃AR model is shown as an example. **(B)** Schematic view of ligand-receptor interaction for the same compound.

This is particularly evident for compounds **6** and **8** (see Figure 4) bearing either a *para*-methoxyphenyl group or a benzyl moiety at R₈, respectively. The increased size of R₈ with respect to

the unsubstituted phenyl ring (compound **4**), together with the lack of the 6-phenyl substituent,

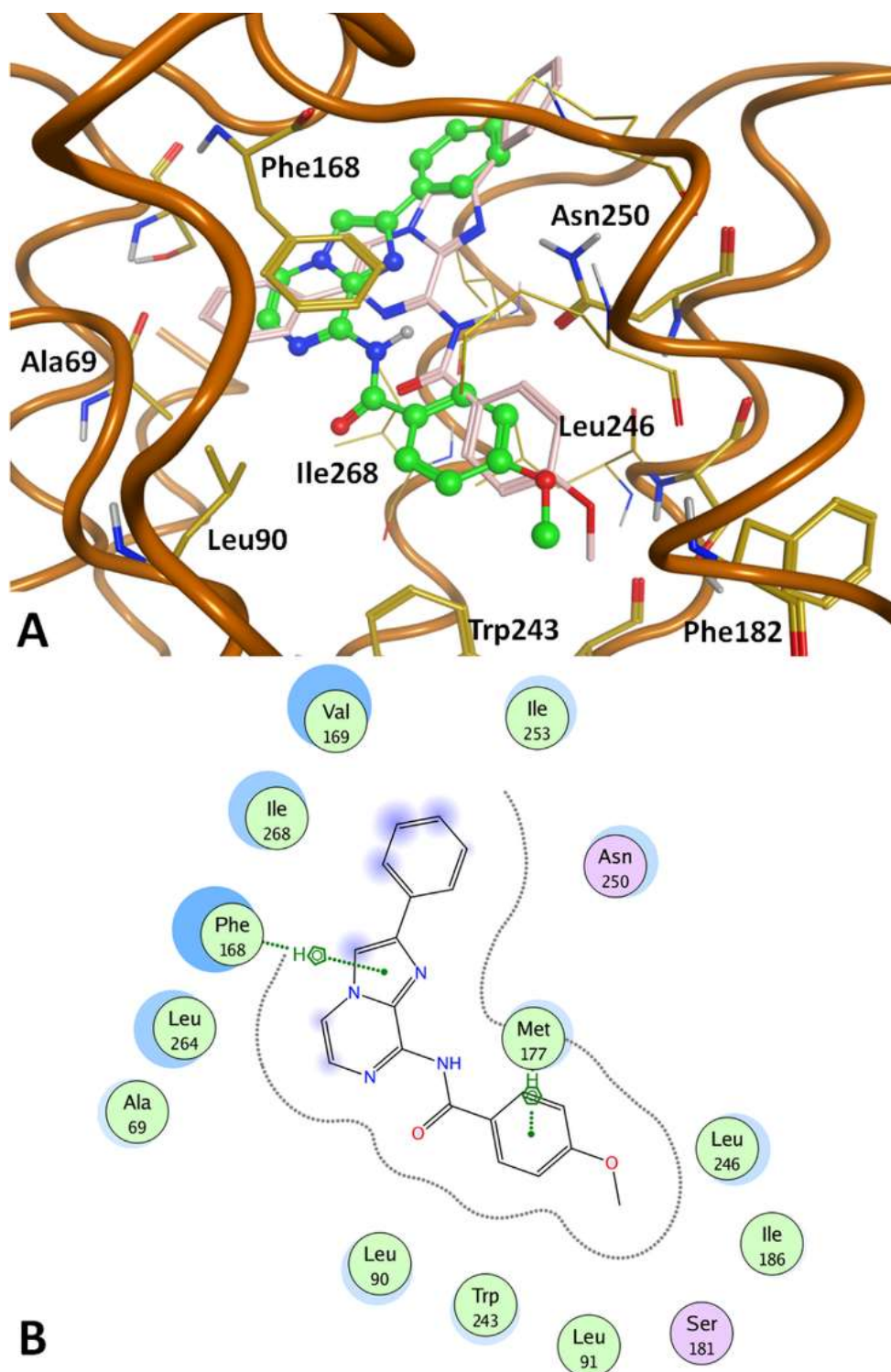


Figure 4. Docking conformations of the 2,8-substituted imidazopyrazine derivatives. (**A**) The binding mode of compound **6** (green) at 3EML-based hA₃AR model is shown as an example. The docking mode of compound **22** (light pink) is shown for comparison. (**B**) Schematic view of ligand-receptor interaction for the same compound.

make the compounds slightly shifted compared to the corresponding binding mode of the 6-phenyl analogues. For this reason, **6** ($K_i = 162$ nM) and **8** ($K_i = 524$ nM) have decreased hA₃ binding affinity compared to **4** that, in contrast, has a K_i value in the nanomolar range ($K_i = 52$ nM). All the other modifications at the 8-substituent result in a loss of affinity.

Regarding the 8-position on the 6-phenyl-imidazopyrazine derivatives, the N⁸-(hetero)arylcarboxyamido substituent is located in the depth of the pocket. The NH function makes an H-bond interaction with the Asn250 (TM6) amide group, while the carbonyl function does not seem to make any direct interaction with the receptor. The aromatic ring is positioned in proximity to TM3 (Leu91), TM5 (Met177 and Ser181), and TM6 (Trp243, Leu246, Ser247, and Asn250) residues, in a region presenting mainly (but not completely) a hydrophobic profile. The replacement of the phenyl ring on the N⁸-carboxyamido chain (**21**, $K_i = 82$ nM) with a more polar substituent like the 3-pyridinyl (compound **29**) or 2-furanyl (derivative **27**) maintains high hA₃ affinity ($K_i = 54$ and 67 nM, respectively). Polar interactions with residues in proximity (i.e. Asn250) can be hypothesized. On the contrary, the replacement with a 2-thienyl is detrimental for the activity (**28**, $K_i = 185$ nM). Substituents at *para*-position of the phenyl ring at R₈ appear to provide higher volume complementarity with the cavity with respect to the unsubstituted aromatic ring, as shown in Figure 5A-B. On the other hand, the different chemical-physical profile of the *para*-substituent takes to a higher or a lower compound affinity for the A₃ AR. In the case of a substituent presenting an H-bond acceptor function, polar contacts are observable with Ser181 and Ser247 side chains. In fact, compound **22** (the most active of the series, $K_i = 25$ nM) has a methoxy substituent at this position and the oxygen atom of this function is located in proximity of Ser181 hydroxyl (Figure 5C). This polar contact is absent for all the other derivatives. On the contrary, the presence on the aromatic ring of hydrophobic substituents like a methyl group (**23**) or a chlorine atom (**24**) leads to a reduced affinity even with respect to the *para*-unsubstituted derivative **21** ($K_i = 223$ and 156 nM, respectively vs **21** $K_i = 82$ nM). Thus, considering that the substituent on the R₈ phenyl ring might interact with the binding site residues in proximity, the effect of the presence of different substituents on this molecule portion was evaluated. This analysis was performed by the use of the *IF-E 6.0* [39] tool retrievable at the SVL exchange service. The script (already successfully used for the analysis of ligand-target interaction for A₃AR [40] and A_{2B}AR [41] agonists) calculates and displays atomic and residue interaction forces as 3D vectors. It also calculates the per-residue interaction energies (values in kcal mol⁻¹), where negative and positive energy values are associated with favorable and unfavorable interactions, respectively. The results (Figure 5D) show that the different substituents provide diverse interactions with the nearby residues.

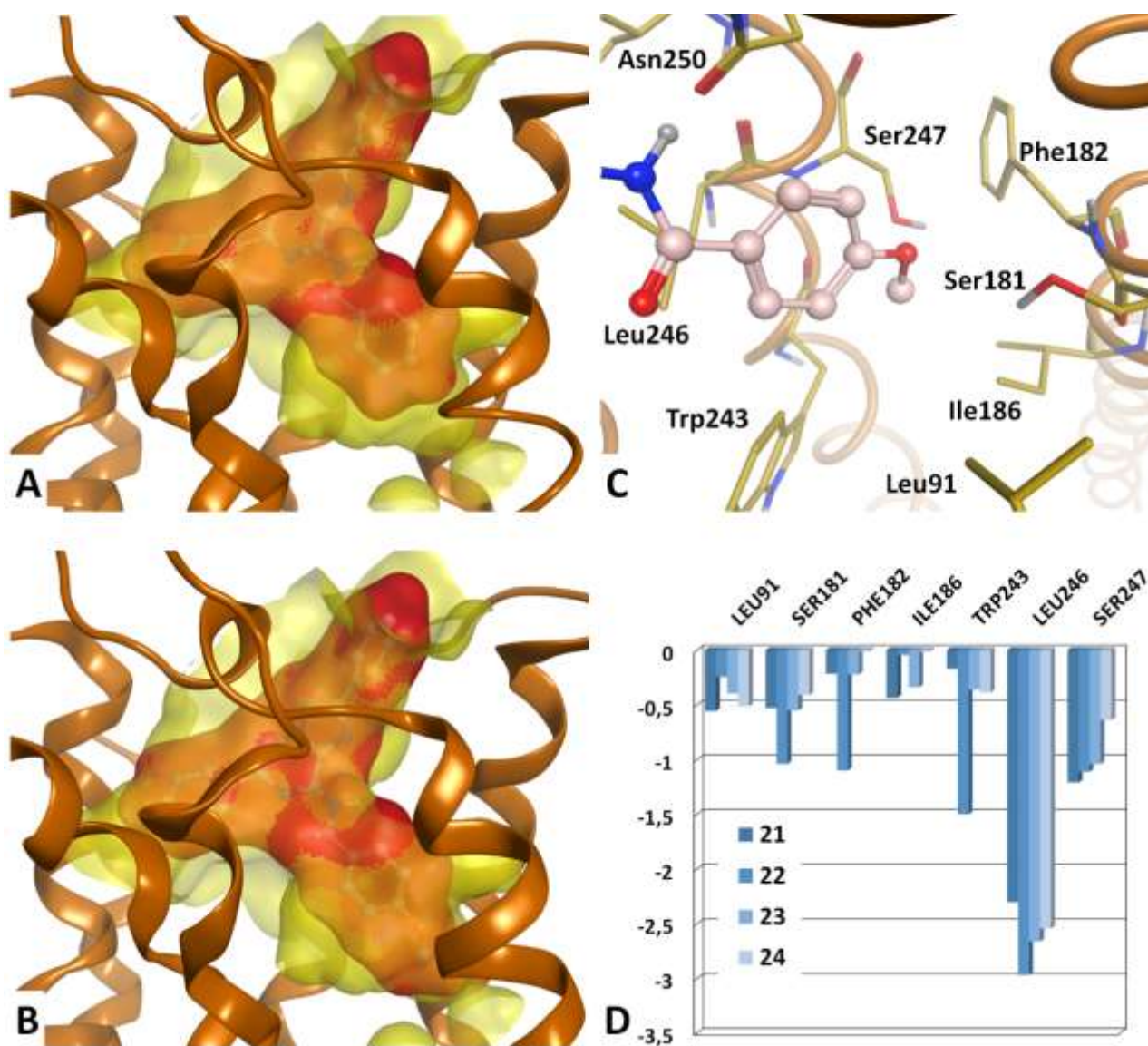


Figure 5. Docking conformation of compounds **21** (A) and **22** (B). Molecular surfaces of both the ligand (dark) and the cavity (light) are represented. Comparison highlights the higher volume complementarity between the cavity and compound **22** with respect to that of compound **21**. (C) Detailed view of the interaction of the 8-substituent of compound **22** with the nearby residues. (D) Ligand–receptor interaction energies (per-residue values) calculated with IF-E 6.0 script. Data of interaction between the receptor and the aromatic group within the 8-substituent are represented. See text for details.

In particular, the methoxy group of **22** increases the interaction with Ser181, Phe182 and Trp243 residues. In the first case, a polar contact is present between the oxygen atom of the ligand and the hydroxyl group of the receptor residue. This interaction is obviously absent in the case of the unsubstituted ligand **21** and for the other two derivatives **23** and **24** presenting, respectively, a methyl group and a chlorine atom as substituents. In the case of Phe182 and Trp243, the methoxy group of **22** makes the methyl function be in proximity of the side chain of these residues, providing an interaction that is almost absent for the other ligands.

In the case of both compounds **5** and **9**, bearing hindering substituents at R₈, the displayed hA₃ binding activity could be explained by hypothesizing an alternative binding mode that allows the two aromatic rings on R₈ to be located within the cavity or possibly to point toward the extracellular space. However, the docking results did not provide a clear depiction for this possible alternative binding mode.

Regarding the 6-phenyl-substituted compound **18**, the lack of the (hetero)aryl substituents on the 8-amino group makes this analogue inactive at the hA₃AR but active at the hA₁ and hA_{2A} ARs. Docking studies at these two receptors were not performed in this investigation, but a possible explanation for this activity could be given by supposing that the binding mode of compound **18** is different from that above described. In this case, the 8-amino group would be allocated in proximity of the Glu172 (EL2) and Asn254 (TM6) of A₁AR or Glu169 (EL2) and Asn252 (TM6) of A_{2A}AR.

5.3. Electrophysiological studies.

Compound **29**, which is one of the most potent and selective hA₃ AR antagonists of this series, was tested in an *in vitro* rat model of cerebral ischemia obtained by oxygen glucose deprivation (OGD) (Figure 6). An important factor in the study of brain ischemia is the generation of anoxic depolarization (AD), a decrease in neuron and glial membrane potential, that is an important parameter of brain tissue integrity contributing to the amount and severity of neuronal damage [42, 43].

In a first series of experiments we characterized the response of evoked field excitatory postsynaptic potentials (fEPSPs) in the CA1 region before and following severe (30-min) OGD, an ischemic insult that under our experimental conditions constantly produces an irreversible loss of synaptic transmission (not shown) even when hippocampal slices were reperfused with oxygenated, glucose-containing aCSF (artificial cerebrospinal fluid). At the same time, we monitored the direct current (d.c.) shift produced by AD during 30-min OGD. The time of the appearance and magnitude of depolarizing d.c. shift, in the absence or in the presence of compound **29** (200 nM), were compared (Figure 6A,B). In agreement with previous findings [8, 11], 30-min OGD elicited the appearance of AD in untreated OGD slices, with a mean latency of 6.3 ± 0.3 minutes ($n = 5$, calculated from the beginning of OGD, panel a) and a mean peak amplitude of -7.5 ± 1.2 mV ($n = 5$, panel b) (Figure 6A and panel a). When OGD was applied in the presence of 200 nM compound **29**, the d.c. shifts were always delayed with a mean latency of 8.2 ± 0.5 minutes ($n = 8$, $P < 0.05$) (Figure 6B and panel a), although the AD amplitude (-7.1 ± 0.8 mV, $n = 8$) was not significantly changed. In agreement with our previous results [11, 12], 7-min OGD completely abolished the fEPSP which did not recover its amplitude after reperfusion in normal oxygenated aCSF (Figure 6C). Seven-min OGD was then applied in the presence of compound **29**.

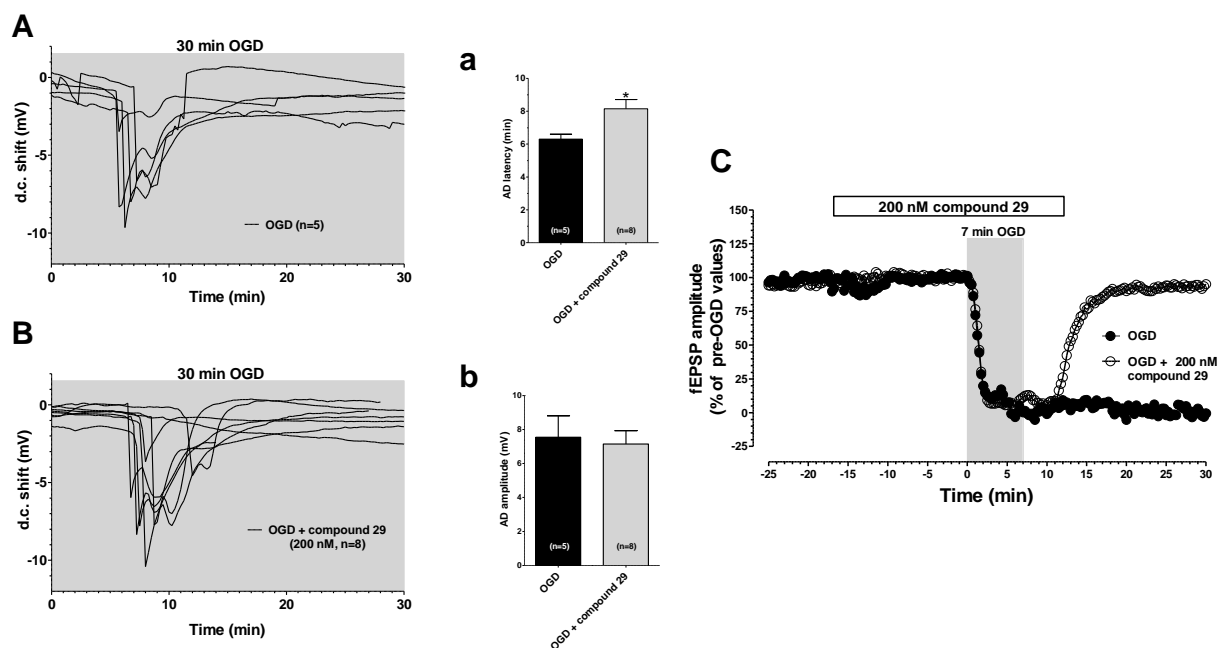


Figure 6. Compound **29** significantly delayed the appearance of AD induced by 30-min OGD in rat hippocampal slices. The graph shows the d.c. shift traces during 30-min OGD in untreated slices (OGD, $n = 5$) (**A**) or in slices treated with compound **29** (200 nM, $n = 8$) (**B**). (**a**) Each column represents the mean (\pm SEM) of AD latency recorded in hippocampal slices during 30-min OGD in the absence (OGD) or in the presence of 200 nM compound **29** (OGD + compound 29, $n=8$). AD was measured from the beginning of OGD insult. Note that compound **29** significantly delayed AD development. $*P < 0.05$, unpaired two-tailed Student's t -test in comparison to untreated OGD slices. (**b**) Each column represents the mean (\pm SEM) of AD amplitude, recorded in hippocampal slices during 30-min OGD, in the absence or in the presence of 200 nM compound **29** (OGD + compound 29, $n=8$). The number (n) of slices tested is reported inside columns. (**C**) Graph shows the time course of 7-min OGD effects on fEPSP amplitude in an untreated OGD slice and in compound **29**-treated OGD slice. Amplitude of fEPSP is expressed as percent of pre-ischemic baseline. Note that, after reperfusion in normal oxygenated aCSF, a significant recovery of fEPSP was found only in compound **29**-treated OGD slices.

As illustrated in Figure 6C, application of compound **29** (200 nM), 15 minutes before, during, and 5 minutes after the OGD insult, provided a significant recovery of fEPSP amplitude within 15-min reperfusion with oxygenated and glucose-containing aCSF. Similar experiments were obtained in three out of the four slices tested (not shown).

Although compound **29** does not show any rA_3 binding affinity (Table 3), it was able to delay AD initiation in a similar manner to those obtained with other structurally related compounds [8, 11, 12]. It is clear that the electrophysiological effect exerted by compound **29** is not mediated through the A_3 AR receptor, but we can hypothesize another mechanism of action that can include an intracellular molecular target.

In any case, compound **29** delays the occurrence of AD and induces a significant recovery of otherwise disrupted neurotransmission acting on fEPSP amplitude. Since AD is an important

determinant of the degree and extent of ischemic damage, compounds that delay the AD initiation may become new therapeutics for counteracting stroke-induced neurodegeneration.

5.4. Conclusions

The present study has led to the identification of some imidazo[1,2-*a*]pyrazines as new hA₃ AR antagonists. In particular, the N⁸-(hetero)arylcarboxyamido substituted compounds **4-14** and **21-30**, bearing a 6-phenyl moiety or not, respectively, show on the whole good hA₃ AR affinity and selectivity *versus* the other ARs. Surprisingly, the 8-amino-6-(hetero)arylimidazopyrazines designed for targeting the hA_{2A} subtype (compounds **31-38**), together with the 6-phenyl analogues **18-20**, turn out to be inactive at the hA_{2A} AR, or endowed with hA₁ or balanced hA₁/hA_{2A} AR affinity in the micromolar range. Molecular docking of the newly hA₃ antagonists allowed us to depict their hypothetical binding mode to our hA₃ receptor model as well as to rationalize the observed SARs. Some derivatives were evaluated for their fluorescent emission properties showing some potentiality but not as fluorescent probes in biological assays. The selected hA₃ AR antagonist 2,6-diphenyl-8-(3-pyridoylamino)imidazo[1,2-*a*]pyrazine **29**, tested in a rat model of cerebral ischemia, delayed the occurrence of AD caused by 30 min OGD in the hippocampus and proved to be significantly effective in recovering the otherwise disrupted neurotransmission, acting on fEPSP amplitude.

6. Experimental section

6.1. Chemistry

Silica gel plates (Merck F₂₅₄) and silica gel 60 (Merck; 70-230 mesh) were used for analytical and preparative TLC, and for column chromatography, respectively. All melting points were determined on a Gallenkamp melting point apparatus. Elemental analyses were performed with a Flash E1112 Thermofinnigan elemental analyzer for C, H, N, and the results were within $\pm 0.4\%$ of the theoretical values. All final compounds revealed a purity not less than 95%. The IR spectra were recorded with a Perkin-Elmer Spectrum RX I spectrometer in Nujol mulls and are expressed in cm⁻¹. The NMR spectra were obtained with a Bruker Avance spectrometer (400 MHz for ¹H NMR, 100 MHz for ¹³C NMR). The chemical shifts are reported in δ (ppm) and are relative to the central peak of the solvent. The coupling constant (*J*) are expressed in Hz. All the exchangeable protons were confirmed by addition of D₂O. The following abbreviations are used: s = singlet, d = doublet, dd = double doublet, t = triplet, m = multiplet, br = broad, and ar = aromatic protons.

6.1.1. General procedure for the synthesis of 2-(hetero)aryl-6,8-dibromoimidazo[1,2-*a*]pyrazines (**39-41**) [30].

A mixture of 3,5-dibromo-2-aminopyrazine [28] (1.2 mmol) and an excess of the suitable α -bromoketone [29] (1.8 mmol) was heated at the convenient temperature (T=100°C, for compounds

39, 41; T=120°C, for **40**) in an open tube until the disappearance of the starting material (TLC monitoring, eluting system dichloromethane/ethyl acetate 6:4). The resulting brown solid was worked up with the minimal amount of ethyl acetate and then collected by filtration.

6.1.1.1. 6,8-Dibromo-2-phenylimidazo[1,2-a]pyrazine (39) [30]. Yield 93%; m.p. > 300 °C (ethanol); ¹H NMR (DMSO-d₆): 7.42 (t, 1H, ar, J = 7.04 Hz), 7.50 (t, 2H, ar, J = 7.72 Hz), 8.04 (d, 2H, ar, J = 7.56 Hz), 8.71 (s, 1H, H-5), 9.00 (s, 1H, H-3); IR: 1645. Anal. C₁₂H₇Br₂N₃ (C, H, N).

6.1.1.2. 6,8-Dibromo-2-(4-methoxyphenyl)imidazo[1,2-a]pyrazine (40). Yield 99%; m.p. 212-216 °C (ethyl acetate/methanol); ¹H NMR (DMSO-d₆): 3.83 (s, 3H, OCH₃), 7.07 (d, 2H, ar, J = 8.88 Hz), 7.99 (d, 2H, ar, J = 8.88 Hz), 8.60 (s, 1H, H-5), 8.96 (s, 1H, H-3); IR: 1643, 1651, 1659. Anal. C₁₃H₉Br₂N₃O (C, H, N).

6.1.1.3. 6,8-Dibromo-2-(furan-2-yl)imidazo[1,2-a]pyrazine (41). Yield 50%; m.p. 216-218 °C (cyclohexane); ¹H NMR (DMSO-d₆): 6.67-6.68 (m, 1H, ar), 7.07-7.08 (m, 1H, ar), 7.86-7.88 (m, 1H, ar), 8.44 (s, 1H, H-5), 8.97 (s, 1H, H-3); ¹³C NMR: 148.12, 144.52, 139.93, 138.46, 131.96, 121.32, 119.24, 113.17, 112.61, 109.51; IR: 1624, 1654, 1685. Anal. C₁₀H₅Br₂N₃O (C, H, N).

6.1.2. General procedure for the synthesis of 6-bromo-2-arylimidazo[1,2-a]pyrazin-8-amines (15-17)

A suspension of the 6,8-dibromo-derivative **39-41** (0.70 mmol) in absolute ethanol (10 mL) saturated with ammonia was heated overnight at 120°C in a sealed tube. The solid that precipitated upon cooling (compounds **15, 16**) was collected by filtration and washed with water. For intermediate **17**, the cooled reaction mixture was diluted with water (30 mL) and extracted with ethyl acetate (30 mL x 2). The organic layer was washed with water (30 mL x 3), anhydriified (Na₂SO₄) and then evaporated under reduced pressure to yield a solid.

6.1.2.1. 6-Bromo-2-phenylimidazo[1,2-a]pyrazin-8-amine (15). Yield 82%; mp 283-285 °C (toluene); ¹H NMR (DMSO-d₆): 7.34 (t, 1H, ar, J = 7.24 Hz), 7.44-7.48 (m, 4H, 2H ar + NH₂), 7.95 (d, 2H, ar, J = 7.60 Hz), 8.02 (s, 1H, H-5), 8.29 (s, 1H, H-3); IR: 1642, 3117, 3170, 3302. Anal. C₁₂H₉BrN₄ (C, H, N).

6.1.2.2. 6-Bromo-2-(4-methoxyphenyl)imidazo[1,2-a]pyrazin-8-amine (16). Yield 27%; m.p. 286-287 °C (ethyl acetate); ¹H NMR (DMSO-d₆): 3.81 (s, 3H, OCH₃), 7.02 (d, 2H, ar, J = 8.56 Hz), 7.39 (br s, 2H, NH₂), 7.88 (d, 2H, ar, J = 8.36 Hz), 8.03 (s, 1H, H-5), 8.18 (s, 1H, H-3); ¹³C NMR: 159.68, 149.25, 144.51, 131.85, 127.40, 126.21, 122.20, 114.66, 111.35, 109.71, 55.65; IR: 1644, 3132, 3165, 3300. Anal. C₁₃H₁₁BrN₄O (C, H, N).

6.1.2.3. 6-Bromo-2-(furan-2-yl)-imidazo[1,2-a]pyrazin-8-amine (17). Yield 61% ; m.p. 235-238 °C (diethyl ether); ¹H NMR (DMSO-d₆): 6.61 (m, 1H, ar), 6.83 (m, 1H, ar), 7.52 (br s, 2H, NH₂), 7.76 (m, 1H, ar), 8.02 (s, 1H, ar), 8.08 (s, 1H, ar); IR: 1643, 3182, 3304. Anal. C₁₀H₇BrN₄O (C, H, N)

6.1.3. General procedure for the synthesis of 2-(hetero)arylimidazo[1,2-a]pyrazin-8-amines (1-3)

10% Pd/C (0.4 g) was cautiously added to a hot solution of the 6-bromo-derivative (**15-17**) (0.63 mmol) in ethanol (50 mL). The mixture was hydrogenated in a Parr apparatus, at 20 psi, for 15 h. The catalyst was filtered off and the solvent was evaporated under reduced pressure. The residue was dissolved in water (60 mL) and the solution was basified with a saturated NaHCO₃ solution. The solid that precipitated was collected and washed with water (compounds **1**, **2**). For compound **3**, upon treatment with saturated NaHCO₃ solution, the resulting aqueous mixture was extracted with ethyl acetate (100 mL) and the organic layer was washed with water (100 mL x 2), anhydridified (Na₂SO₄) and evaporated to small volume under reduced pressure. The white solid that precipitated was collected by suction.

6.1.3.1. 2-Phenylimidazo[1,2-a]pyrazin-8-amine (1). Yield 77%; m.p. 208-209 °C (diethyl ether/petroleum ether); ¹H NMR (DMSO-d₆): 6.88 (br s, 2H, NH₂), 7.21 (d, 1H, H-6, J = 4.56 Hz), 7.32 (t, 1H, ar, J = 7.32 Hz), 7.44-7.48 (m, 2H, ar), 7.76 (d, 1H, H-5, J = 4.56 Hz), 7.97 (d, 2H, ar, J = 7.32 Hz), 8.33 (s, 1H, H-3); IR: 1630, 3130, 3273, 3444. Anal. C₁₂H₁₀N₄ (C, H, N).

6.1.3.2. 2-(4-Methoxyphenyl)imidazo[1,2-a]pyrazin-8-amine (2). Yield 44%; m.p. 249-250 °C (ethyl acetate); ¹H NMR (DMSO-d₆): 3.81 (s, 3H, OCH₃), 6.83 (br s, 2H, NH₂), 7.02 (d, 2H, ar, J = 8.68 Hz), 7.18 (d, 1H, H-6, J = 4.56 Hz), 7.73 (d, 1H, H-5, J = 4.56 Hz), 7.89 (d, 2H, ar, J = 8.68 Hz), 8.21 (s, 1H, H-3); IR: 1627, 3142, 3283, 3445. Anal. C₁₃H₁₂N₄O (C, H, N).

6.1.3.3. 2-(Furan-2-yl)imidazo[1,2-a]pyrazin-8-amine (3). Yield 42%; m.p. 225-227 °C (ethyl acetate); ¹H NMR (DMSO-d₆): 6.61 (br s, 1H, ar), 6.80 (br s, 1H, ar), 6.93 (s, 2H, NH₂), 7.22 (d, 1H, H-6, J = 4.56 Hz), 7.77-7.76 (m, 2H, H-5 + ar), 8.13 (s, 1H, H-3); IR: 3302, 3143. Anal. C₁₀H₈N₄O (C, H, N).

6.1.4. Synthesis of 8-benzoylamino-2-phenylimidazo[1,2-a]pyrazine (4) and 8-dibenzoylamino-2-phenylimidazo[1,2-a]pyrazine (5)

A solution of the 8-amino derivative **1** (0.47 mmol) and benzoyl chloride (0.57 mmol) in anhydrous tetrahydrofuran (2 mL) and anhydrous pyridine (3 mL) was heated at reflux for 6 h. After cooling, the reaction mixture was diluted with water (20 mL) and ice (50 g) was added. The suspension was stirred at room temperature for 30 min. The solid which precipitated (compounds **4** and **5**, 1:2 mixture, ¹H NMR valuation) was collected by filtration and washed with water. Compounds **4** and **5** were separated by silica gel column chromatography, eluting system dichloromethane/ethyl acetate 1:1. The first and the central eluates were evaporated under reduced pressure to give compound **4** and **5**, respectively.

6.1.4.1. 8-Benzoylamino-2-phenylimidazo[1,2-a]pyrazine (4). Yield 27%; m.p. 179-180 °C (diethyl ether/petroleum ether); ¹H NMR (DMSO-d₆): 7.37 (t, 1H, ar, J = 7.36 Hz), 7.47 (t, 2H, ar, J = 7.32 Hz), 7.58 (t, 2H, ar, J = 7.64 Hz), 7.66 (t, 1H, ar, J = 7.40 Hz), 7.74 (br s, 1H, H-6), 8.0 (d, 2H, ar, J

= 7.24 Hz), 8.09 (d, 2H, ar, J = 6.88 Hz), 8.48 (br s, 1H, H-5), 8.63 (s, 1H, H-3), 10.87 (br s, 1H, NH); ¹³C NMR: 166.21, 145.77, 144.00, 136.50, 134.29, 133.36, 132.68, 129.29, 129.03, 128.88, 128.58, 127.79, 126.50, 118.96, 112.21; IR: 1627, 1700, 3391. Anal. C₁₉H₁₄N₄O (C, H, N) .

6.1.4.2. 8-Dibenzoylamino-2-phenylimidazo[1,2-a]pyrazine (5). Yield 41%; m.p. 219-220 °C dec. (ethanol); ¹H NMR (DMSO-d₆): 7.38-7.40 (m, 1H, ar), 7.47-7.49 (m, 6H, ar), 7.59 (t, 2H, ar, J = 7.12 Hz), 7.68 (d, 1H, H-6), J = 4.36 Hz), 7.83 (d, 4H, ar, J = 7.56 Hz), 7.93 (d, 2H, ar, J = 7.56 Hz), 8.56 (d, 1H, H-5, J = 4.40 Hz), 8.68 (s, 1H, H-3); IR: 1697, 3396. Anal. C₂₆H₁₈N₄O₂ (C, H, N) .

6.1.5. Synthesis of 8-dibenzoylamino-2-phenylimidazo[1,2-a]pyrazine (5)

A solution of the 8-amino derivative **1** (0.67 mmol) and benzoyl chloride (6.7 mmol) in anhydrous pyridine (3 mL) was heated at reflux for 3 h. After cooling, the reaction mixture was diluted with water (20 mL) and treated with 6N HCl to pH 2. The resulting suspension was extracted with ethyl acetate (15 mL x 3) and the organic layers were washed with water (20 mL x 2), anhydriified (Na₂SO₄) and evaporated under reduced pressure. The crude product was purified by silica gel column chromatography, eluting system cyclohexane/ethyl acetate 1:1. Yield 47%.

6.1.6. General procedure for the synthesis of 8-amido-substituted 2-(hetero)arylimidazo[1,2-a]pyrazine derivatives (6-13)

A mixture of the imidazopyrazin-8-amino derivative **1-3** (1.43 mmol), the suitable carboxylic acid (10 mmol), 1-(3-(dimethylamino)-propyl)-3-ethyl-carbodiimide hydrochloride (10 mmol), 1-hydroxy-benzotriazole hydrochloride (10 mmol), triethylamine (21.4 mmol), and 4-(dimethylamino)pyridine (0.14 mmol) in anhydrous dimethylformamide (3 mL) was stirred at room temperature until the disappearance of the starting material. The reaction mixture was diluted with water (50 mL). For compounds **6**, **7**, **9** and **11** the resulting precipitate was collected by filtration, washed with water and purified by silica gel column chromatography (eluting system dichloromethane/ethyl acetate/methanol 7:2:1 for compounds **6**, **7** or dichloromethane/ethyl acetate 1:1 for compound **9**), or directly by crystallization (compound **11**). In the case of derivative **8**, **10**, **12** and **13**, the aqueous suspension obtained after dilution of the reaction mixture was extracted with ethyl acetate (20mL x 3). The organic layers were anhydriified (Na₂SO₄) and evaporated under reduced pressure to yield a solid which was purified by crystallization (compounds **12**, **13**) or by silica gel column chromatography (eluting system dichloromethane/ethyl acetate/methanol 6:3:1 for compound **8**, or 7:2:1 for compound **10**).

6.1.6.1. 8-(4-Methoxybenzoyl)amino-2-phenylimidazo[1,2-a]pyrazine (6). Yield 75%; m.p. 197-198 °C (cyclohexane/ethyl acetate); ¹H NMR (DMSO-d₆): 3.88 (s, 3H, OCH₃), 7.11 (d, 2H, ar, J = 8.24 Hz), 7.38 (t, 1H, ar, J = 8.02 Hz), 7.47 (t, 2H, ar, J = 7.80 Hz), 7.74 (br s, 1H, H-6), 7.99 (d, 2H, ar, J

= 7.76 Hz), 8.06 (d, 2H, ar, J = 8.16 Hz), 8.48 (s, 1H, H-5, J = 4.36 Hz), 8.62 (s, 1H, H-3), 10.68 (s, 1H, NH); IR: 1643, 1695, 3237. Anal. C₂₀H₁₆N₄O₂ (C, H, N).

6.1.6.2. 8-(4-Methylbenzoylamino)-2-phenylimidazo[1,2-a]pyrazine (**7**). Yield 59%; m.p. 202-203 °C (diethyl ether); ¹H NMR (DMSO-d₆): 2.43 (s, 3H, CH₃), 7.38 (m, 3H, ar), 7.47 (t, 2H, ar, J = 7.12 Hz), 7.74 (d, 1H, H-6, J = 4.56 Hz), 7.99-8.01 (m, 4H, ar), 8.48 (d, 1H, H-5, J = 4.32 Hz), 8.62 (s, 1H, H-3), 10.75 (br s, 1H, NH); IR : 1703, 3103, 3407. Anal. C₂₀H₁₆N₄O (C, H, N)

6.1.6.3. 8-(Phenylacetyl)amino-2-phenylimidazo[1,2-a]pyrazine (**8**). Yield 19%; m.p. 177-179 °C (diethyl ether); ¹H NMR (DMSO-d₆): 3.96 (s, 2H, CH₂), 7.27 (t, 1H, ar, J = 7.32 Hz), 7.34-7.43 (m, 5H, ar), 7.51 (t, 2H, ar, J = 7.44 Hz), 7.63 (d, 1H, H-6, J = 4.56 Hz), 8.04 (d, 2H, ar, J = 7.64 Hz), 8.36 (d, 1H, H-5, J = 4.48 Hz), 8.58 (s, 1H, H-3), 10.54 (br s, 1H, NH); IR: 1670, 3357. Anal. C₂₀H₁₆N₄O (C, H, N).

6.1.6.4. 8-Diphenylacetylamino-2-phenylimidazo[1,2-a]pyrazine (**9**). Yield 62%; m.p. 90-92 °C (cyclohexane/ethyl acetate); ¹H NMR (DMSO-d₆): 5.67 (s, 1H, CH), 7.27-7.32 (m, 2H, ar), 7.36-7.42 (m, 5H, ar), 7.47-7.51 (m, 6H, ar), 7.65 (d, 1H, H-6, J = 4.52 Hz), 8.04 (d, 2H, ar, J = 7.32 Hz), 8.39 (d, 1H, H-5, J = 4.52 Hz), 8.58 (s, 1H, H-3), 10.84 (s, 1H, NH); IR: 1701. Anal. C₂₆H₂₀N₄O (C, H, N).

6.1.6.5. 8-(2-Furoylamino)-2-phenylimidazo[1,2-a]pyrazine (**10**). Yield 22%; m.p. 199-200 °C (diethyl ether); ¹H NMR (DMSO-d₆): 6.77 (br s, 1H, ar), 7.39 (t, 1H, ar, J = 7.16 Hz), 7.47-7.50 (m, 3H, ar), 7.73 (d, 1H, H-6, J = 4.08 Hz), 8.01-8.04 (m, 3H, ar), 8.47 (d, 1H, H-5, J = 4.0 Hz), 8.63 (s, 1H, H-3), 10.58 (br s, 1H, NH); IR: 1692, 3383. Anal. C₁₇H₁₂N₄O₂ (C, H, N).

6.1.6.6. 2-Phenyl-8-(3-pyridoylamino)-imidazo[1,2-a]pyrazine (**11**). Yield 53%; m.p. 163-164 °C (ethanol); ¹H NMR (DMSO-d₆): 7.37 (t, 1H, ar, J = 7.36 Hz), 7.47 (t, 2H, ar, J = 7.36 Hz), 7.60-7.62 (m, 1H, ar), 7.76 (br s, 1H, H-6), 8.01 (d, 2H, ar, J = 7.40 Hz), 8.39 (br s, 1H, ar), 8.52 (br s, 1H, H-5), 8.65 (s, 1H, H-3), 8.82 (d, 1H, H-5, J = 3.80 Hz), 9.19 (br s, 1H, ar), 11.20 (br s, 1H, NH); IR: 1702, 3100, 3246. Anal. C₁₈H₁₃N₅O (C, H, N).

6.1.6.7. 8-Benzoylamino-2-(4-methoxyphenyl)imidazo[1,2-a]pyrazine (**12**). Yield 20%; m.p. 135-136 °C dec. (ethyl acetate); ¹H NMR (DMSO-d₆): 3.81 (s, 3H, OCH₃), 7.05 (d, 2H, ar, J = 8.72 Hz), 7.57-7.61 (m, 2H, ar), 7.66-7.68 (m, 1H, ar), 7.78 (d, 1H, H-6), 7.95 (d, 2H, ar, J = 8.64 Hz), 8.09 (d, 2H, ar, J = 7.36 Hz), 8.51 (d, 1H, H-5, J = 4.36 Hz), 8.59 (s, 1H, H-3), 10.83 (s, 1H, NH); IR: 1685, 1702, 3400. Anal. C₂₀H₁₆N₄O₂ (C, H, N).

6.1.6.8. 8-Benzoylamino-2-(furan-2-yl)-imidazo[1,2-a]pyrazine (**13**). Yield 30%; m.p. 209-210 °C (cyclohexane/ethyl acetate); ¹H NMR (DMSO-d₆): 6.62-6.63 (m, 1H, ar), 6.93 (d, 1H, ar, J = 3.36 Hz), 7.58 (t, 2H, ar, J = 7.4 Hz), 7.68-7.64 (m, 1H, ar), 7.77 (d, 1H, H-6, J = 4.52 Hz), 7.80-7.79 (m, 1H, ar), 8.06 (d, 2H, ar), 8.42 (s, 1H, H-3), 8.51 (d, 1H, H-5, J = 4.52 Hz), 10.89 (s, 1H, NH); ¹³C

NMR: 166.26, 148.94, 143.88, 138.00, 136.57, 134.16, 132.70, 128.99, 128.62, 127.92, 119.05, 112.38, 111.66, 108.34; IR: 1683, 3182. C₁₇H₁₂N₄O₂ (C, H, N).

6.1.7. Synthesis of 2-phenyl-8-(3-phenylureido)imidazo[1,2-a]pirazine (**14**)

Phenylisocyanate (0.95 mmol) was added to an equimolar amount of the 8-amino derivative **1** in anhydrous dichloromethane (6 ml). The reaction mixture was stirred at room temperature for 20 h. The solid that precipitated was collected by filtration. Yield: 83%; m.p. 222-224 °C (ethanol); ¹H NMR (DMSO-d₆): 7.10 (t, 1H, ar, J = 7.40 Hz), 7.34-7.42 (m, 3H, ar), 7.48 (m, 2H, ar), 7.63-7.65 (m, 3H, ar + H-6), 8.07 (d, 2H, ar, J = 7.24 Hz), 8.24 (d, 1H, H-5, J = 4.68 Hz), 8.59 (s, 1H, H-3), 9.20 (s, 1H, NH), 11.60 (s, 1H, NH); IR: 3407, 3139, 1701. Anal. C₁₉H₁₅N₅O (C, H, N).

6.1.8. General procedure for the synthesis of 2-(hetero)aryl-6-phenylimidazo[1,2-a]pyrazin-8-amines (**18-20**)

The suitable 6-bromo-2-(hetero)aryl substituted derivative **15-17** (0.86 mmol) was added to a mixture of Na₂CO₃ (8.64 mmol), tetrakis (0.08 mmol) and phenyl boronic acid (1.29 mmol) in 1,2-dimethoxyethane/water 3:1 (15 mL). The reaction mixture was heated at 85 °C under nitrogen atmosphere until the disappearance of the starting material (TLC monitoring, eluting system cyclohexane/ethyl acetate 6:4). After dilution with water (250 mL) a solid precipitated which was collected by suction (compounds **18** and **20**) or extracted with ethyl acetate (50 mL x 3). The organic layer was washed with water (100 mL x 2), anhydriified (Na₂SO₄) and evaporated under reduced pressure to give a solid (compound **19**). In the case of derivatives **19**, **20** the crude product was purified by silica gel column chromatography, eluting system cyclohexane/ethyl acetate 6:4 (compound **19**) or dichloromethane/methanol 9:1 (compound **20**).

6.1.8.1. 2,6-Diphenylimidazo[1,2-a]pyrazin-8-amine (**18**). Yield 98%; m.p. 207-208 °C dec. (ethanol); ¹H NMR (DMSO-d₆): 7.08 (s, 2H, NH₂), 7.33-7.38 (m, 2H, ar), 7.44-7.49 (m, 4H, ar), 7.96-8.01 (m, 4H, ar), 8.34 (s, 1H, H-3), 8.39 (s, 1H, H-5); IR: 1643, 3181, 3304. C₁₈H₁₄N₄ (C, H, N).

6.1.8.2. 2-(4-Methoxyphenyl)-6-phenyl-imidazo[1,2-a]pyrazin-8-amine (**19**). Yield 80%; m.p. 196-198 (ethanol); ¹H NMR (DMSO-d₆): 3.81 (s, 3H, OCH₃); 6.99 (s, 2H, NH₂); 7.04 (d, 2H, ar, J = 8.80 Hz); 7.35 (t, 1H, ar, J = 7.30 Hz); 7.45 (t, 2H, ar, J = 7.60 Hz); 7.91-7.97 (m, 4H, ar); 8.23 (s, 1H, H-3); 8.37 (s, 1H, H-5); IR: 1654, 3325. C₁₉H₁₆N₄O (C, H, N).

6.1.8.3. 2-(Furan-2-yl)-6-phenylimidazo[1,2-a]pyrazin-8-amine (**20**). Yield 50%; m.p. 201-202 °C (petroleum ether/ethyl ether) ¹H NMR (DMSO-d₆): 6.62-6.63 (m, 1H, ar), 6.84-6.86 (m, 1H, ar), 7.09 (s, 2H, NH₂), 7.36 (t, 1H, ar, J = 6.60 Hz), 7.46 (t, 2H, ar, J = 7.44 Hz), 7.77 (s, 1H, ar), 7.94 (d, 2H, ar, J = 7.84 Hz), 8.13 (s, 1H, H-3), 8.40 (s, 1H, H-5); IR: 3309, 3159. Anal. C₁₆H₁₂N₄O (C, H, N).

6.1.9. General procedure for the synthesis of 8-amido-substituted 2-(hetero)aryl-6-phenylimidazo[1,2-a]pyrazine derivatives (**21-30**)

A solution of the 8-amino derivative **18**, **19** (0.7 mmol) and the suitable (hetero)aroyl chloride (0.77 mmol) in anhydrous pyridine (4 mL) was heated at reflux until the disappearance of the starting material (TLC monitoring, eluting system dichloromethane/ethyl acetate 7:3). After cooling, the reaction mixture was diluted with water (20 mL) and treated with 6N HCl to pH 3. The resulting suspension was extracted with ethyl acetate (20 mL x 3) and the organic layers were washed with water (50 mL x 2), then with a saturated NaHCO₃ solution (50 mL) and finally with water (50 mL x 2). After anhydricification (Na₂SO₄) the organic solvent was evaporated under reduced pressure.

The crude product was purified by preparative silica gel thin layer chromatography 1:1 (eluting system dichloromethane for compound **21**, dichloromethane/ethyl acetate 9:1, compound **23**, dichloromethane/acetonitrile, compound **27** and dichloromethane/ethyl acetate 9.5:0.5 for derivative **28**, **30**) or directly by crystallization (**24**, **26**). Derivatives **22**, **25** were obtained as an oily residue that was worked up with a little amount of diethyl ether/petroleum ether 1:1. A solid precipitated which was collected by filtration and recrystallized.

6.1.9.1. 8-Benzoylamino-2,6-diphenylimidazo[1,2-a]pyrazine (21). Yield 20%; m.p. 124-125 °C dec. (cyclohexane/ethyl acetate); ¹H NMR (DMSO-d₆): 7.37-7.54 (m, 6H, ar), 7.58-7.62 (m, 2H, ar), 7.67 (m, 1H, ar), 8.04 (m, 4H, ar), 8.10 (d, 2H, ar, J = 7.64 Hz), 8.61 (s, 1H, H-3), 9.10 (s, 1H, H-5), 10.97 (s, 1H, NH); IR: 1705, 3401. Anal. C₂₅H₁₈N₄O (C, H, N).

6.1.9.2. 8-(4-Methoxybenzoyl)amino-2,6-diphenylimidazo[1,2-a]pyrazine (22). Yield 28%; m.p. 114-115 °C dec. (cyclohexane/ethyl acetate); ¹H NMR (DMSO-d₆): 3.89 (s, 3H, OCH₃), 7.13 (d, 2H, ar, J = 8.76 Hz), 7.39-7.54 (m, 6H, ar), 8.04 (t, 4H, ar, J = 8.04 Hz), 8.10 (d, 2H, ar, J = 8.76 Hz), 8.60 (s, 1H, H-3), 9.08 (s, 1H, H-5), 10.78 (s, 1H, NH); IR: 1693, 3385. Anal. C₂₆H₂₀N₄O₂ (C, H, N).

6.1.9.3. 8-(4-Methylbenzoyl)amino-2,6-diphenylimidazo[1,2-a]pyrazine (23). Yield 14%; m.p. 110-111 °C (cyclohexane/ethyl acetate); ¹H NMR (DMSO-d₆): 2.44 (s, 3H, CH₃), 7.38-7.54 (m, 8H, ar), 8.00-8.05 (m, 6H, ar), 8.61 (s, 1H, H-3), 9.10 (s, 1H, H-5), 10.89 (s, 1H, NH); IR: 1679, 3434. Anal. C₂₆H₂₀N₄O (C, H, N).

6.1.9.4. 8-(4-Chlorobenzoyl)amino-2,6-diphenylimidazo[1,2-a]pyrazine (24). Yield 12%; m.p. 217-218 °C dec (ethyl acetate); ¹H NMR (DMSO-d₆): 7.37-7.54 (m, 6H, ar), 7.67 (d, 2H, ar, J = 7.4 Hz), 8.03 (t, 4H, ar, J = 8.04 Hz), 8.11 (d, 2H, ar, J = 7.72), 8.61 (s, 1H, H-3), 9.10 (s, 1H, H-5), 11.11 (s, 1H, NH); IR (cm⁻¹): 1667, 3356. Anal. C₂₅H₁₇ClN₄O (C, H, N).

6.1.9.5. 8-(4-Fluorobenzoyl)amino-2,6-diphenylimidazo[1,2-a]pyrazine (25). Yield 17%; m.p. 195-196 °C dec. cyclohexane/ethylacetate; ¹H NMR (DMSO-d₆): 7.39-7.54 (m, 8H, ar), 8.04 (d, 4H, ar, J = 7.72 Hz), 8.18 (m, 2H, ar), 8.61 (s, 1H, H-3), 9.10 (s, 1H, H-5), 11.04 (s, 1H, NH); ¹³C NMR: 166.20, 165.48, 163.71, 146.30, 142.94, 136.72, 136.39, 135.59, 133.30, 131.53, 131.44, 130.85,

129.26, 128.98, 128.94, 126.52, 126.29, 116.12, 115.90, 114.93, 112.69; IR: 1713, 3403. Anal. $C_{25}H_{17}FN_4O$ (C, H, N).

6.1.9.6. 8-[bis(4-Fluorobenzoyl)amino]-2,6-diphenylimidazo[1,2-a]pyrazine (**26**). Yield 24 %; m.p. 274-275 °C; 1H NMR (DMSO- d_6): 7.33-7.49 (m, 10H, ar), 7.70 (d, 2H, ar, $J = 7.20$ Hz), 7.95-7.98 (m, 6H, ar), 8.66 (s, 1H, H-3), 9.16 (s, 1H, H-5); IR: 1699, 3380. Anal. $C_{32}H_{20}F_2N_4O_2$ (C, H, N, O).

6.1.9.7. 8-(2-Furanoyl)amino-2,6-diphenylimidazo[1,2-a]pyrazine (**27**). Yield 28%; m.p. 202-203 °C; 1H NMR (DMSO- d_6): 6.78-6.80 (m, 1H, ar), 7.40-7.45 (m, 2H, ar), 7.48-7.55 (m, 5H, ar), 8.05-8.08 (m, 5H, ar), 8.61 (s, 1H, H-3) 9.08 (s, 1H, H-5), 10.65 (s, 1H, NH); IR: 1696, 3372. Anal. $C_{23}H_{16}N_4O_2$ (C, H, N).

6.1.9.8. 2,6-Diphenyl-8-(2-thenoyl)aminoimidazo[1,2-a]pyrazine (**28**). Yield 72% ; m.p. 206-207 °C; 1H NMR (DMSO- d_6): 7.30 (t, 1H, ar, $J = 4.44$ Hz), 7.37-7.55 (m, 6H, ar), 7.96 (d, 1H, ar, $J = 4.76$ Hz), 8.04-8.07 (m, 4H, ar), 8.19 (br s, 1H, ar), 8.61 (s, 1H, H-3), 9.10 (s, 1H, H-5), 11.07 (s, 1H, NH); IR: 1669, 3457. Anal. $C_{23}H_{16}N_4OS$ (C, H, N).

6.1.9.9. 8-Benzoylamino-2-(4-methoxy)phenyl-6-phenylimidazo[1,2-a]pyrazine (**30**). Yield 26%; m.p. 136-138 °C (ethyl acetate); 1H NMR (DMSO- d_6): 3.81 (s, 3H, OCH_3), 7.04 (d, 2H, ar, $J = 8.60$ Hz), 7.41 (t, 1H, ar, $J = 7.0$ Hz), 7.51 (t, 2H, ar, $J = 7.60$ Hz), 7.59 (t, 2H, ar, $J = 7.78$ Hz), 7.67 (t, 1H, ar, $J = 7.24$), 7.97 (d, 2H, ar, $J = 8.64$ Hz), 8.03 (d, 2H, ar, $J = 7.84$ Hz), 8.10 (d, 2H, ar, $J = 8.60$ Hz), 8.50 (s, 1H, H-3), 9.06 (s, 1H, H-5), 10.92 (s, 1H, NH); IR : 1679, 3445. Anal. $C_{26}H_{20}N_4O_2$ (C, H, N).

6.1.10. Synthesis of 2,6-diphenyl-8-(3-pyridoylamino)imidazo[1,2-a]pyrazine (**29**)

A solution of the 8-amino derivative **18** (0.7 mmol) and 3-pyridoyl chloride (0.77 mmol) in anhydrous pyridine (4 mL) was heated at reflux for 3h. After cooling, the reaction mixture was diluted with water (60 mL) and then extracted with ethyl acetate (20 mL x 5). The organic layers were washed with water (50 mL x 3), then anhydriified (Na_2SO_4) and evaporated under reduced pressure. Yield 28%; m.p. 233-234 °C dec. (ethyl acetate); 1H NMR (DMSO- d_6): 7.39-7.53 (m, 7H, ar), 7.61-7.65 (m, 1H, ar), 8.00-8.05 (m, 5H, ar), 8.41 (d, 1H, ar, $J = 7.96$ Hz), 8.62 (s, 1H, H-3), 8.83 (d, 1H, ar, $J = 3.36$ Hz), 9.11 (s, 1H, H-5), 9.21 (s, 1H, ar), 11.30 (s, 1H, NH); ^{13}C NMR: 165.42, 153.06, 149.66, 146.37, 142.62, 136.66, 136.41, 136.33, 135.38, 133.28, 130.21, 129.30, 129.27, 128.97, 126.54, 126.27, 124.09, 115.02, 112.77; IR: 1684. Anal. $C_{25}H_{19}N_5O_2$ (C, H, N).

6.1.11. Synthesis of 3-(2-phenylacetamido)phenylboronic acid (**42**)

A solution of 2-phenylacetyl chloride (2.92 mmol) in anhydrous tetrahydrofuran (4 mL) was drop by drop added at room temperature to a solution of 3-aminophenylboronic acid (1.46 mmol) in anhydrous tetrahydrofuran (4 mL) containing triethylamine (7.3 mmol). After stirring at room temperature for 1 h, the reaction mixture was diluted with water (15 mL) and stirred again for 30 min.

Then, the suspension was extracted with ethyl acetate (20 mL x 3) and the dried organic layers (Na₂SO₄) were evaporated under reduced pressure. The crude product was pure enough to be used without further purification. Yield 48%; ¹H NMR (DMSO-d₆) δ: 3.63 (s, 2H, CH₂), 7.23-7.36 (m, 6H, ar), 7.46 (d, 1H, ar, J = 7.32 Hz), 7.71 (d, 1H, ar, J = 8.00 Hz), 7.83 (s, 1H, ar), 8.04 (s, 2H, 2OH), 10.09 (s, 1H, NH).

6.1.12. General procedure for the synthesis of 2,6-(hetero)arylimidazo[1,2-a]pyrazin-8-amines (**31-38**)

The 6-bromo-2-(hetero)aryl substituted derivative **15**, **17** (0.86 mmol) was added to a mixture of Na₂CO₃ (8.64 mmol), tetrakis (0.08 mmol) and the suitable (hetero)arylboronic acid (1.29 mmol) (compound **42** or commercially available boronic acid) in 1,2-dimethoxyethane/water 3:1 (15 mL). The reaction mixture was heated at 85 °C under nitrogen until the disappearance of the starting material (TLC monitoring). In the case of compounds **31**, **33**, **36-38** after dilution with water (60 mL) a solid precipitated which was collected by suction and treated as described below. The crude product was purified by silica gel column chromatography eluting systems dichloromethane/ethyl acetate 8:2 (compound **31**), cyclohexane/ethylacetate 1:1 (compound **33**), dichloromethane/methanol 9:1 (compound **38**) and with a gradient silica gel column for compound **37** (eluting system dichloromethane/ethyl acetate 7:3 for the first eluates, and then in the ratio 1:1 for the second crop). For derivative **32**, after dilution with water (60 mL) of the reaction mixture and separation of the precipitate, the aqueous solution was extracted with ethyl acetate (20 mL x 2). The organic layers were anhydriified (Na₂SO₄) and evaporated under reduced pressure to yield a crude product which was worked up with diethyl ether (2 mL) and collected by filtration. The resulting solid and the precipitate collectetd above were purified by silica gel column chromatography, eluting system cyclohexane/ethyl acetate 1:1: Derivative **36**, after subsequent hot washings with methanol (2 mL x 2), was separated by suction and washed with diethyl ether (2 mL).

Compound **34** was isolated after evaporation at reduced pressure of the reaction mixture, treatment with water (15 mL) of the crude residue, acidification of the resulting suspension with glacial acetic acid, extraction of the resulting aqueous suspension with ethyl acetate (20 mL x 3) and evaporation of the dried (Na₂SO₄) organic layers. For compound **35** the reaction mixture was diluted with water (60 mL) and extracted with ethyl acetate (15 mL x 3); then, the dried (Na₂SO₄) organic layers were evaporated under reduced pressure to give a white solid.

6.1.12.1. 6-(3-Methoxyphenyl)-2-phenylimidazo[1,2-a]pyrazin-8-amine (**31**). Yield 51%; m.p. 198-200 °C (cyclohexane/ethyl acetate); ¹H NMR (DMSO-d₆): 3.84 (s, 3H, OCH₃), 6.93 (m, 1H, ar), 7.06 (s, 2H, NH₂), 7.33-7.39 (m, 2H, ar), 7.47 (t, 2H, ar, J = 7.52 Hz), 7.53-7.55 (m, 2H, ar), 8.01 (d, 2H,

ar, J = 7.60 Hz), 8.33 (s, 1H, H-3), 8.41 (s, 1H, H-5); IR: 1643, 3158, 3307. Anal. C₁₉H₁₆N₄O (C, H, N).

6.1.12.2. 6-(4-Methoxyphenyl)-2-phenylimidazo[1,2-a]pyrazin-8-amine (**32**). Yield 29%; m.p. 219-221 °C (ethyl acetate); ¹H NMR (DMSO-d₆): 3.81 (s, 3H, OCH₃), 7.01-7.03 (m, 4H, ar + NH₂), 7.35 (t, 1H, ar, J = 7.20 Hz), 7.47 (t, 2H, ar, J = 7.40 Hz), 7.90 (d, 2H, ar, J = 8.80 Hz), 7.99 (d, 2H, ar, J = 7.32 Hz), 8.29 (s, 1H, H-3), 8.31 (s, 1H, H-5); IR: 1640, 3181. Anal. C₁₉H₁₆N₄O (C, H, N).

6.1.12.3. 6-(4-Chlorophenyl)-2-phenylimidazo[1,2-a]pyrazin-8-amine (**33**). Yield 27%; m.p. 223-225 °C (diethyl ether); ¹H NMR (DMSO-d₆): 7.13 (s, 2H, NH₂), 7.35 (t, 1H, ar, J = 7.52 Hz), 7.47 (t, 2H, ar, J = 7.36 Hz), 7.52 (d, 2H, ar, J = 8.56 Hz), 7.99-8.01 (m, 4H, ar), 8.34 (s, 1H, H-3), 8.45 (s, 1H, H-5); IR: 1640, 3381. Anal. C₁₈H₁₃ClN₄ (C, H, N).

6.1.12.4. 3-(8-Amino-2-phenylimidazo[1,2-a]pyrazin-6-yl)benzoic acid (**34**) Yield 30%; m.p. 197-199 °C dec. (methanol); ¹H NMR (DMSO-d₆): 7.14 (s, 2H, NH₂), 7.35 (t, 1H, ar, J = 7.52 Hz), 7.48 (t, 2H, ar, J = 7.60 Hz), 7.58 (t, 1H, ar, J = 7.68 Hz), 7.93 (d, 1H, ar, J = 7.56 Hz), 8.00 (d, 2H, ar, J = 8.08 Hz), 8.18 (d, 1H, ar, J = 7.60 Hz), 8.35 (s, 1H, H-3), 8.51 (s, 1H, H-5), 8.61 (s, 1H, ar); IR: 3398, 1680. Anal. C₁₉H₁₄N₄O₂ (C, H, N).

6.1.12.5. N-[3-(8-Amino-2-phenylimidazo[1,2-a]pyrazin-6-yl)phenyl]-2-phenylacetamide (**35**). Yield 42%; m.p. 204-205 °C (ethyl acetate); ¹H NMR (DMSO-d₆): 3.68 (s, 2H, CH₂), 7.03 (s, 2H, NH₂), 7.26 (t, 1H, ar, J = 6.84 Hz), 7.33-7.39 (m, 6H, ar), 7.47 (t, 2H, ar, J = 7.60 Hz), 7.60 (t, 2H, ar, J = 7.76 Hz), 7.99 (d, 2H, ar, J = 7.52 Hz), 8.21 (s, 1H, ar), 8.29 (s, 1H, H-3), 8.36 (s, 1H, H-5), 10.29 (s, 1H, NH); IR: 1640, 1955, 3292, 3372. Anal. C₂₆H₂₁N₅O (C, H, N).

6.1.12.6. 6-[4-(Benzyloxy)phenyl]-2-phenylimidazo[1,2-a]pyrazin-8-amine (**36**). Yield 26%; m.p. 211-212 °C (ethyl acetate); ¹H NMR (DMSO-d₆): 5.16 (s, 2H, CH₂), 7.03 (s, 2H, NH₂), 7.10 (d, 2H, ar, J = 8.0 Hz), 7.35-7.48 (m, 8H, ar), 7.90 (d, 2H, ar, J = 7.68 Hz), 7.99 (d, 2H, ar, J = 7.72 Hz), 8.30 (s, 1H, ar), 8.31 (s, 1H, ar); IR: 1648, 3267. Anal. C₂₅H₂₀N₄O (C, H, N).

6.1.12.7. 6-(Furan-2-yl)-2-phenylimidazo[1,2-a]pyrazin-8-amine (**37**). Yield 50%; m.p. 244-246 °C (methanol); ¹H NMR (DMSO-d₆): 6.61 (m, 1H, ar), 6.8 (m, 1H, ar), 7.1 (s, 2H, NH₂), 7.35 (t, 1H, ar, J = 7.56 Hz), 7.47 (t, 2H, ar, J = 7.56 Hz), 7.74 (s, 1H, ar), 7.97 (d, 2H, ar, J = 8.0 Hz), 8.16 (s, 1H, H-3), 8.38 (s, 1H, H-5); IR: 1648, 3151, 3308. Anal. C₁₆H₁₂N₄O (C, H, N, O).

6.1.12.8. 2,6-(Furan-2-yl)-imidazo[1,2-a]pyrazin-8-amine (**38**). Yield 63%; m.p. 256-257 °C (diethyl ether); ¹H NMR (DMSO-d₆): 6.58-6.62 (m, 2H, ar), 6.78-6.82 (m, 2H, ar), 7.14 (s, 2H, NH₂), 7.74 (s, 1H, ar), 7.76 (s, 1H, ar), 8.19 (s, 2H, H-3 + H-5); IR: 3314, 3152. Anal. C₁₄H₁₀N₄O₂ (C, H, N).

6.2. Fluorescence studies.

6.2.1. Materials and instrumentation.

Uvasol ethanol for spectroscopy, chloroform, 2-aminopyridine and H₂SO₄ were from Merck (Germany). Quinine sulfate was from Laboratori Angelini (Italy). MilliQ water was used to prepare sulphuric acid diluted solutions throughout this work. Fluorescence and absorbance measurements were performed in 10mm pathlength quartz cuvettes.

Fluorescence spectra were obtained using a Jasco FP-750 Spectrofluorimeter controlled by Jasco software.

The UV-visible adsorption spectra and absorbance measurements were obtained using a EVOLUTION 220 UV-visible spectrophotometer controlled by Thermoinsight software (Thermo Scientific).

6.2.2. Fluorescence spectroscopy.

Emission spectra of the different compounds were determined in CHCl₃ and in some case in EtOH solution. In all the experiments the excitation and emission bandpass was set at 5nm, with "medium" sensitivity and response. The emission spectra were obtained from 250 to 600 nm with the excitation set at the appropriate λ_{ex} . The excitation spectra were obtained from 220 and 500 with the emission being recorded at the appropriate wavelength.

Cross-calibration was performed using quinine sulfate and 2-Aminopyridine as standard compounds. This was achieved by calculating the quantum yield of each standard compound relative to the other. The value of the quantum yield of each standard compound obtained by experiments should match the literature values. The match is generally considered valid and acceptable if the data obtained is of good quality (i.e. good linearity with a zero intercept) and the experimental quantum yields match their literature counterparts within $\pm 10\%$.

6.2.3. Fluorescence quantum yield evaluation.

The most reliable method for recording fluorescence quantum yield (Φ) is the comparative method [44] which involves the use of well characterized standard samples with known Φ values. The quantum yield is calculated using the slope of the line determined from the calibration plot of the absorbance against the integrated fluorescence intensities.

The overall procedure can be summarized as follows:

1. The UV-vis absorbance spectrum of the solvent background for the chosen sample is recorded.
2. Fluorescence spectrum of the same solution in the 10 mm fluorescence cuvette was recorded and the integrated fluorescence intensity was calculated
3. The above mentioned steps were repeated for five solutions with increasing concentrations of the chosen sample; there will be six solutions, corresponding to absorbances at the excitation wavelength of 0/solvent (blank), 0.02, 0.04, 0.06, 0.08, 0.10) [45].

4. A graph of integrated fluorescence intensity vs absorbance is plotted. The results should be a straight line with gradient m , and intercept = 0.

The gradients of the graphs obtained as described above are proportional to the quantum yield of the different samples. Absolute values are calculated using the standard samples which have a fixed and known fluorescence quantum yield value, according to the following equation:

$$\Phi_x = \Phi_{ST} \left(\frac{\text{Grad}_x}{\text{Grad}_{ST}} \right) \left(\frac{\eta_{ST}^2}{\eta_x^2} \right)$$

Where the subscripts ST and x denote standard and test respectively, Φ is the fluorescence quantum yield, Grad the gradient from the plot of integrated fluorescence intensity vs absorbance, and η the refractive index of the solvent.

The gradient for each sample is proportional to that sample's fluorescence quantum yield. Conversion into an absolute quantum yield is achieved through the equation given in the text.

6.3. Molecular modeling studies

6.3.1. Computational methodologies

Homology modeling, energy minimization, and docking studies were carried out using Molecular Operating Environment (MOE, version 2010.10) suite [36]. Manual docking and Monte Carlo studies of the MRS 1220 binding mode were done using MOE and Schrodinger Macromodel (ver. 8.0) [46] with Schrodinger Maestro interface. Compounds docking analyses were then performed with MOE. All ligand structures were optimized using RHF/AM1 semiempirical calculations and the software package MOPAC implemented in MOE was utilized for these calculations [38].

6.3.2. Homology modeling of the human A₃AR.

The homology model of the hA₃AR was built using the X-ray structure of the inverse agonist-bound hA_{2A}AR as template (pdb code: 3EML; 2.6-Å resolution [33]). A multiple alignment of the AR primary sequences was built within MOE as preliminary step. The boundaries identified from the used X-ray crystal structure of hA_{2A}AR were then applied for the corresponding sequences of the TM helices of the hA₃AR. The missing loop domains were built by the loop search method implemented in MOE. Once the heavy atoms were modeled, all hydrogen atoms were added, and the protein coordinates were then minimized with MOE using the AMBER99 force field [47]. The minimizations were performed by steepest descent steps followed by conjugate gradient minimization until the RMS gradient of the potential energy was less than 0.05 kJ mol⁻¹ Å⁻¹. Reliability and quality of the model was checked using the Protein Geometry Monitor application within MOE, which provides a variety of stereochemical measurements for inspection of the structural quality in a given protein, like

backbone bond lengths, angles and dihedrals, Ramachandran ϕ - ψ dihedral plots, and sidechain rotamer and nonbonded contact quality.

6.3.3. Preliminary docking analysis with MRS 1220.

A preliminary docking analysis was performed by manually docking MRS 1220 structure within the hA₃AR model binding site. The obtained hA₃AR-MRS 1220 complex was then subjected to energy minimization refinement and to Monte Carlo analysis to explore the favorable binding conformations. This analysis was conducted by Monte Carlo Conformational Search protocol implemented in Schrodinger Macromodel. The input structure consisted of the ligand and a shell of receptor amino acids within the specified distance (6 Å) from the ligand. A second external shell of all the residues within a distance of 8 Å from the first shell was kept fixed. During the Monte Carlo conformational searching, the input structure was modified by random changes in user-specified torsion angles (for all input structure residues), and molecular position (for the ligand). Hence, the ligand was left free to be continuously re-oriented within the binding site and the conformation of both ligand and internal shell residues could be explored and reciprocally relaxed. The method consisted of 10,000 Conformational Search steps with MMFF94s force field [48-54]. The best hA₃AR-MRS 1220 complex was saved and subjected to energy minimization with the same protocol as above. This protocol was recently used to prepare hA₃AR models for docking and dynamics studies of nucleoside agonists at the same receptor [40,55].

6.3.4. Molecular docking analysis.

All compound structures were docked into the binding site of the hA₃AR model using the MOE Dock tool. This method is divided into a number of stages: *Conformational Analysis of ligands*. The algorithm generated conformations from a single 3D conformation by conducting a systematic search. In this way, all combinations of angles were created for each ligand. *Placement*. A collection of poses was generated from the pool of ligand conformations using Triangle Matcher placement method. Poses were generated by superposition of ligand atom triplets and triplet points in the receptor binding site. The receptor site points are alpha sphere centers which represent locations of tight packing. At each iteration a random conformation was selected, a random triplet of ligand atoms and a random triplet of alpha sphere centers were used to determine the pose. *Scoring*. Poses generated by the placement methodology were scored using two available methods implemented in MOE, the *London dG* scoring function which estimates the free energy of binding of the ligand from a given pose, and *Affinity dG* scoring which estimates the enthalpic contribution to the free energy of binding. The top 30 poses for each ligand were output in a MOE database.

6.3.5 Post Docking analysis

The five top-score docking poses of each compound were then subjected to AMBER99 force field energy minimization until the RMS gradient of the potential energy was less than $0.05 \text{ kJ mol}^{-1} \text{ \AA}^{-1}$. Receptor residues within 6 \AA distance from the ligand were left free to move, while the remaining receptor coordinates were kept fixed. AMBER99 partial charges of receptor and MOPAC output partial charges of ligands were utilized. Once the compound-binding site energy minimization was completed, receptor coordinates were fixed and a second energy minimization stage was performed leaving free to move only compound atoms. MMFF94 force field was applied. For each compound, the minimized docking poses were then rescored using *London dG* and *Affinity dG* scoring functions and the *dock-pK_i* predictor. The latter tool allows estimating the pK_i for each ligand using the “scoring.svl” script retrievable at the SVL exchange service (Chemical Computing Group, Inc. SVL exchange: <http://svl.chemcomp.com>). The algorithm is based on an empirical scoring function consisting of a directional hydrogen-bonding term, a directional hydrophobic interaction term, and an entropic term (ligand rotatable bonds immobilized in binding). For each compound, the top-score docking poses according to at least two out of three scoring functions were selected for final ligand-target interaction analysis.

The interactions between the ligands and the receptors binding site were analysed by using the *IF-E 6.0* tool [39] retrievable at the SVL exchange service. The program calculates and displays the atomic and residue interaction forces as 3D vectors. It also calculates the per-residue interaction energies, where negative and positive energy values (expressed as kcal mol^{-1}) are associated to favourable and unfavourable interactions, respectively. A shell of residues contained within a 10 \AA distance from ligand were considered for this analysis.

7.1. Pharmacology.

7.1.1. Human cloned A₁, A_{2A} and A₃ AR binding assay

All synthesized compounds were tested to evaluate their affinity at hA₁, hA_{2A} and hA₃ adenosine receptors. Displacement experiments of [³H]DPCPX (1 nM) to hA₁ CHO membranes (50 µg of protein/assay) and at least six to eight different concentrations of antagonists for 120 min at 25 °C in 50 mM Tris HCl buffer pH 7.4 were performed [56]. Non specific binding was determined in the presence of 1 µM of DPCPX ($\leq 10\%$ of the total binding). Binding of [³H]ZM-241385 (1 nM) to hA_{2A}CHO membranes (50 µg of protein/assay) was performed using 50 mM Tris HCl buffer, 10 mM MgCl₂ pH 7.4 and at least six to eight different concentrations of antagonists studied for an incubation time of 60 min at 4 °C [57]. Non specific binding was determined in the presence of 1 µM ZM241385 and was about 20% of total binding. Competition binding experiments to hA₃ CHO or rA₃ membranes

(50 µg of protein/assay) and 0.5 nM [¹²⁵I]AB-MECA, 50 mM Tris HCl buffer, 10 mM MgCl₂, 1 mM EDTA, pH 7.4, with at least six to eight different concentrations of examined ligands for 120 min at 4 °C, were conducted [58]. Non-specific binding was defined as binding in the presence of 1 µM AB-MECA and was about 20% of total binding. Bound and free radioactivity were separated by filtering the assay mixture through Whatman GF/B glass fiber filters using a Brandel cell harvester. The filter bound radioactivity was counted by Scintillation Counter Packard Tri Carb 2810 TR with an efficiency of 62%.

7.1.2. Measurement of cyclic AMP levels in CHO cells transfected with hA_{2B} or hA₃ ARs.

CHO cells transfected with hA_{2B} or hA₃ ARs were washed with phosphate-buffered saline, detached with trypsin and centrifuged for 10 min at 200 g. The pellet containing the CHO cells (1×10⁶ cells /assay) was suspended in 0.5 ml of incubation mixture (mM): NaCl 15, KCl 0.27, NaH₂PO₄ 0.037, MgSO₄ 0.1, CaCl₂ 0.1, Hepes 0.01, MgCl₂ 1, glucose 0.5, pH 7.4 at 37 °C, 2 IU/ml adenosine deaminase and 4-(3-butoxy-4-methoxybenzyl)-2-imidazolidinone (Ro 20-1724) as phosphodiesterase inhibitor and preincubated for 10 min in a shaking bath at 37 °C. The potency of antagonists to A_{2B} ARs was determined by antagonism of NECA (200 nM)-induced stimulation of cyclic AMP levels. In addition, the potency of antagonists to A₃ receptors was determined in the presence of forskolin 1 µM and Cl-IB-MECA (100 nM) that mediated inhibition of cyclic AMP levels. The reaction was terminated by the addition of cold 6% trichloroacetic acid (TCA). The TCA suspension was centrifuged at 2000 g for 10 min at 4 °C and the supernatant was extracted four times with water saturated diethyl ether. The final aqueous solution was tested for cyclic AMP levels by a competition protein binding assay. Samples of cyclic AMP standard (0-10 pmoles) were added to each test tube containing [³H] cyclic AMP and the incubation buffer (trizma base 0.1 M, aminophylline 8.0 mM, 2-mercaptoethanol 6.0 mM, pH 7.4). The binding protein prepared from beef adrenals, was added to the samples previously incubated at 4 °C for 150 min, and after the addition of charcoal were centrifuged at 2000 g for 10 min. The clear supernatant was counted in a Scintillation Counter Packard Tri Carb 2810 TR with an efficiency of 58% [59].

7.1.3. Rat A₃ receptor binding.

Selected compounds were tested for evaluating their affinity at ratA₃ adenosine receptors expressed in HEK293 cells (Perkin-Elmer, Boston, USA). Competition binding experiments to rA₃ HEK membranes (10 µg of protein/assay) and 0.5 nM [¹²⁵I]AB-MECA, 50 mM Tris-HCl buffer, 10 mM MgCl₂, 1 mM EDTA, pH 7.4 and at least 3–4 different concentrations of examined ligands for 120 min at 25 °C [58]. Non-specific binding was defined as binding in the presence of 1 µM AB-MECA and was about 20% of total binding. Bound and free radioactivity were separated by filtering the assay mixture through Whatman GF/B glass fiber filters by using a Brandel cell harvester. The filter

bound radioactivity was counted by Scintillation Counter Packard Tri Carb 2500 TR with an efficiency of 58%.

7.1.4. Data analysis

The protein concentration was determined according to a Bio-Rad method with bovine albumin as a standard reference [58]. Inhibitory binding constant (K_i) values were calculated from those of IC_{50} according to Cheng & Prusoff equation $K_i = IC_{50}/(1+[C^*]/K_D^*)$, where $[C^*]$ is the concentration of the radioligand and K_D^* its dissociation constant [59]. EC_{50} and IC_{50} values obtained in cyclic AMP assay were calculated by non linear regression analysis using the equation for a sigmoid concentration-response curve (Graph-PAD Prism, San Diego, CA, U.S.A) [59].

8.1. Electrophysiological assays.

8.1.1. Slice Preparation.

All animal procedures were conducted according to the European Community Guidelines for Animal Care, DL 116/92, application of the European Communities Council Directive (86/609/EEC). Experiments were approved by the Institutional Animal Care and Use Committee (IACUC) of the University of Florence and performed according to the Italian Law on Animal Welfare (DL 116/92). All efforts were made to minimize animal sufferings and to use only the number of animals necessary to produce reliable scientific data. Experiments were carried out on acute hippocampal slices [60], prepared from male Wistar rats (Harlan Italy; Udine Italy, 150-200 g body weight). Animals were killed with a guillotine under anesthesia with isoflurane (Baxter, Rome, Italy) and their hippocampi were rapidly removed and placed in ice-cold oxygenated (95% O_2 -5% CO_2) aCSF of the following composition (mM): NaCl 125, KCl 3, NaH_2PO_4 1.25, $MgSO_4$ 1, $CaCl_2$ 2, $NaHCO_3$ 25, and D-glucose 10. Slices (400 μm thick) were cut using a McIlwain tissue chopper (The Mickle Laboratory, Engineering, Co. Ltd., Gomshall, U.K.) and kept in oxygenated aCSF for at least 1 h at room temperature. A single slice was then placed on a nylon mesh, completely submerged in a small chamber (0.8 ml), and superfused with oxygenated aCSF (31-32 $^{\circ}C$) at a constant flow rate of 1.5-1.8 mL min⁻¹. The treated solutions reached the preparation in 60 s, and this delay was taken into account in our calculations.

8.1.2. Extracellular Recording.

Test pulses (80 μs , 0.066 Hz) were delivered through a bipolar nichrome electrode positioned in the stratum radiatum. Evoked extracellular potentials were recorded with glass microelectrodes (2-10 M Ω , Harvard Apparatus LTD, Edenbridge, U.K.) filled with 150 mM NaCl and placed in the CA1 region of the stratum radiatum. Responses were amplified (BM 622, Mangoni, Pisa, Italy), digitized (sample rate, 33.33 kHz), and stored for later analysis with LTP (version 2.30D) program [61].

Stimulus-response curves were obtained by gradual increases in stimulus strength at the beginning of each experiment, when a stable baseline of evoked response was reached. The test stimulus pulse was then adjusted to produce a fEPSP whose amplitude was 40% to 50% of the maximum and was kept constant throughout the experiment. The fEPSP amplitude was routinely measured and expressed as the percentage of the average amplitude of the potentials measured during the 5 min preceding exposure of the hippocampal slices to OGD. In some experiments, both the amplitude and initial fEPSP slope were quantified, but because no appreciable differences between these two parameters were observed in drug effect and OGD, only the amplitude measurement is expressed in the Figures. Simultaneously with fEPSP amplitude, AD, induced by 7 or 30 min OGD, was recorded as negative extracellular d.c. shifts. The d.c. potential is an extracellular recording considered to provide an index of the polarization of cells surrounding the tip of the glass electrode [62]. AD latency, expressed in min, was calculated from the beginning of OGD; AD amplitude, expressed in mV, was calculated at the maximal negativity peak. In the text and bar graphs, AD amplitude values were expressed as positive values.

8.1.3. Application of OGD and Drugs.

OGD was obtained by perfusing the slice with aCSF without glucose and gassed with nitrogen (95% N₂ and 5% CO₂) [63]. This caused a drop in pO₂ in the recording chamber from ~500 mmHg (normoxia) to a range of 35-75 mmHg (after 7 min of OGD) [6]. At the end of the ischemic period, the slice was again superfused with normal, glucose containing, oxygenated aCSF. Throughout this paper, the terms ‘untreated OGD slices’ or ‘treated OGD slices’ refer to hippocampal slices in which OGD episodes of different duration were applied in the absence or in the presence of compound **29**, respectively. The selective A₃ adenosine receptor antagonist was applied 15 min before, during, and 5 min after OGD. The compound was made up to a 100 μ M stock solution in dimethyl sulfoxide (DMSO). These stock solutions were aliquoted, stored at -20 °C, and diluted in aCSF before use. The final concentration of DMSO (0.05% and 0.01% in aCSF) used in our experiments did not affect either fEPSP amplitude or the depression of synaptic potentials induced by OGD (not shown).

8.1.4. Statistics.

Data were analyzed using Prism 3.02 software (Graphpad Software, San Diego, CA). All numerical data are expressed as the mean (SEM). Data were tested for statistical significance with the unpaired Student's *t* test. A value of $p < 0.05$ was considered significant.

Acknowledgements

The synthetic work was supported by a grant of the University of Florence and the Italian Ministry for University and Research (MIUR, PRIN 2010-2011, 20103779_04 project) and the Ente Cassa di

Risparmio di Firenze (2013.0664A2202.3926 project). The molecular modeling work has been carried out with financial support from the University of Camerino, Italy, and the Italian Ministry for University and Research, Rome, Italy.

References.

- [1] B.B. Fredholm, A.P. IJzerman, K.A. Jacobson, J. Linden, C.E. Muller, International union of Pharmacology LXXXI. Nomenclature and classification of adenosine receptors. An up date. *Pharmacol. Rev.* 63 (2011) 1-34.
- [2] K.A Jacobson, L.J.S. Knutsen, P1 and P2 purine and pyrimidine receptor ligands. In: *Purinergic and Pyrimidinergic Signalling*, Abbracchio, M. P., Williams, M., Eds, Handbook of Experimental Pharmacology, Vol. 151/1, Berlin 2001, 129-175.
- [3] V. Ralevic, G. Burnstock, Receptors for purines and pyrimidines. *Pharmacol. Rev.* 50 (1998) 413-492.
- [4] C.E. Müller , K.A. Jacobson, Recent developments in adenosine receptor ligands and their potential as novel drugs, *Biochimica et Biophysica Acta* 1808 (2011) 1290–1308.
- [5] P.A. Borea, K. Varani, F. Vincenzi, P.G. Baraldi, M.A. Tabrizi, S. Merighi, S. Gessi, The A₃ adenosine receptor: history and perspectives, *Pharmacol. Rev.* 67 (2015) 74-102.
- [6] A.M. Pugliese, S. Latini, R. Corradetti, F. Pedata, Brief, repeated, oxygen-glucose deprivation episodes protect neurotransmission from a longer ischemic episode in the in vitro hippocampus: role of adenosine receptors. *Br. J. Pharmacol.* 140 (2003) 305–314.
- [7] A.M. Pugliese, E. Coppi, R. Volpini, G. Cristalli, R. Corradetti, L.S. Jeong, K.A. Jacobson, F. Pedata, Adenosine receptors in health and disease, *Biochem. Pharmacol.* 74 (2007) 768-779.
- [8] V. Colotta, D. Catarzi, F. Varano, F. Capelli, O. Lenzi, G. Filacchioni, C. Martini, L. Trincavelli, O. Ciampi, A.M. Pugliese, F. Pedata, A. Schiesaro, E. Morizzo, S. Moro, Arylpyrazolo[3,4-c]quinoline derivatives as potent and selective human A₃ adenosine receptor antagonists. Synthesis, pharmacological evaluation and ligand-receptor modeling studies, *J. Med. Chem.* 50 (2007) 4061-4074.
- [9] F. Pedata, A.M. Pugliese, E. Coppi, I. Dettori, G. Maraula, L. Cellai, A. Melani, Adenosine A_{2A} receptors modulate acute injury and neuroinflammation in brain ischemia, *Mediators. Inflamm.* 2014:805198.10.1155/2014/805198.

- [10] D. Catarzi, V. Colotta, F. Varano, O. Lenzi, G. Filacchioni, L. Trincavelli, C. Martini, C., C. Montopoli, S. Moro, 1,2,4-Triazolo[1,5-a]quinoxaline as a versatile tool for the design of selective human A₃ adenosine receptor antagonists: synthesis, biological evaluation and molecular modeling studies of 2-(hetero)aryl- and 2-carboxy-substituted derivatives, *J. Med. Chem.* 48 (2005) 7932-7945.
- [11] V. Colotta, D. Catarzi, F. Varano, O. Lenzi, G. Filacchioni, C. Martini, L. Trincavelli, O. Ciampi, C. Traini, A.M. Pugliese, F. Pedata, E. Morizzo, S. Moro, Synthesis, ligand-receptor modeling studies and pharmacological evaluation of novel 4-modified-2-aryl-1,2,4-triazolo[4,3-a]quinoxalin-1-one derivatives as potent and selective human A₃ Adenosine Receptor Antagonists, *Bioorg. Med. Chem.* 16 (2008) 6086-6102.
- [12] V. Colotta, O. Lenzi, D. Catarzi, F. Varano, G. Filacchioni, C. Martini, L. Trincavelli, O. Ciampi, A.M. Pugliese, C. Traini, F. Pedata, A. Schiesaro, E. Morizzo, S. Moro, Pyrido[2,3-*e*]-1,2,4-triazolo[4,3-a]pyrazin-1-one as a new scaffold to develop potent and selective human A₃ adenosine receptor antagonists. Synthesis, pharmacological evaluation and ligand-receptor modeling studies, *J. Med. Chem.* 52 (2009) 2407-2419.
- [13] D. Catarzi, V. Colotta, F. Varano, D. Poli, L. Squarcialupi, G. Filacchioni, K. Varani, F. Vincenzi, P. A. Borea, D. Dal Ben, C. Lambertucci, G. Cristalli, Pyrazolo[1,5-*c*]quinazoline derivatives and their simplified analogues as adenosine receptor antagonists. Synthesis, structure-affinity relationships and molecular modeling studies. *Bioorg. Med. Chem.* 21 (2013) 283-294.
- [14] E. Morizzo, F. Capelli, O. Lenzi, D. Catarzi, F. Varano, G. Filacchioni, F. Vincenzi, K. Varani, P. A. Borea, V. Colotta, S. Moro, Scouting human A₃ adenosine receptor antagonist binding mode using a molecular simplification approach: from triazoloquinoxaline to a pyrimidine skeleton as a key study, *J. Med. Chem.* 50 (2007) 6596-6606.
- [15] D. Poli, D. Catarzi, V. Colotta, F. Varano, G. Filacchioni, S. Daniele, L. Trincavelli, C. Martini, S. Paoletta, S. Moro, The identification of the 2-phenylphthalazin-1(2H)-one scaffold as a new decorable core skeleton for the design of potent and selective human A₃ adenosine receptor antagonists, *J. Med. Chem.* 54 (2011) 2102-2113.
- [16] L. Squarcialupi, V. Colotta, D. Catarzi, F. Varano, G. Filacchioni, K. Varani, F. Vincenzi, P.A. Borea, C. Ghelardini, L. Di Cesare Mannelli, A. Ciancetta, S. Moro, 2-Arylpyrazolo[4,3-*d*]pyrimidin-7-amino derivatives as new potent and selective human A₃ adenosine receptor antagonists. Molecular modeling studies and pharmacological evaluation, *J. Med. Chem.* 56 (2013) 2256-2269.
- [17] D. Catarzi, F. Varano, D. Poli, L. Squarcialupi, M. Betti, L. Trincavelli, C. Martini, D. Dal Ben, A. Thomas, R. Volpini, V. Colotta. 1,2,4-Triazolo[1,5-a]quinoxaline derivatives and their simplified analogues as adenosine A₃ receptor antagonists. Synthesis, structure-affinity relationships and molecular modeling studies. *Bioorg. Med. Chem.* 23 (2015) 9-21.

- [18] F. Varano, D. Catarzi, L. Squarcialupi, M. Betti, F. Vincenzi, A. Ravani, K. Varani, D. Dal Ben, A. Thomas, R. Volpini, V. Colotta. Exploring the 7-oxo-thiazolo[5,4-d]pyrimidine core for the design of new human adenosine A₃ receptor antagonists. Synthesis, molecular modeling studies and pharmacological evaluation. *Eur. J. Med. Chem.* 96 (2015) 105-121.
- [19] L. Squarcialupi, V. Colotta, D. Catarzi, F. Varano, M. Betti, K. Varani, F. Vincenzi, P. A. Borea, N. Porta, A. Ciancetta, S. Moro, 7-Amino-2-phenylpyrazolo[4,3-d]pyrimidine derivatives: structural investigation at the 5-position to target human A₁ and A_{2A} adenosine receptors. Molecular modeling and pharmacological studies. *Eur. J. Med. Chem.* 84 (2014) 614-627.
- [20] S. Taliani, M. Bellandi, C. La Motta, F. Da Settimo, A₃ receptor ligands: past, present and future trends, *Curr. Top. Med. Chem.* 10 (2010) 942-975.
- [21] S. Federico, A. Ciancetta, N. Porta, S. Redenti, G. Pastorin, B. Cacciari, K. N. Klotz, S. Moro, G. Spalluto. 5,7-Disubstituted-[1,2,4]triazolo[1,5-a][1,3,5]triazines as pharmacological tools to explore the antagonist selectivity profiles toward adenosine receptors. *Eur. J. Med. Chem.* 108, (2016) 529-541.
- [22] G. Venkatesan, P. Paira, S. L. Cheong, S. Federico, K. N. Klotz, G. Spalluto, G. Pastorin. •A facile and novel synthesis of N2-, C6-substituted pyrazolo[3,4-d]pyrimidine-4 carboxylate derivatives as adenosine receptor antagonists. *Eur. J. Med. Chem.* 92 (2015) 784-798.
- [23] L. Squarcialupi, M. Falsini, D. Catarzi, F. Varano, M. Betti, K. Varani, F. Vincenzi, D. Dal Ben, C. Lambertucci, R. Volpini, V. Colotta. Exploring the 2- and 5-positions of the pyrazolo[4,3-d]pyrimidin-7-amino scaffold to target human A₁ and A_{2A} adenosine receptors. *Bioorg. Med. Chem.* 108 (2016) 117-133.
- [24] D. Preti, P. G. Baraldi, A. R. Moorman, P. A. Borea, K. Varani, History and perspectives of A_{2A} adenosine receptor antagonists as potential therapeutic agents. *Med. Res. Rev.* 35 (2015) 790-848.
- [25] J.J. Matasi, J.P. Caldwell, H. Zhang, A. Fawzi, M.E. Cohen-Williams, G.B. Varty, D.B. Tulshian, 2-(2-Furanyl)-7-phenyl[1,2,4]triazolo[1,5-c]pyrimidin-5-amine analogs: Highly potent, orally active, adenosine A_{2A} antagonists. Part 1. *Bioorg. Med. Chem. Letters* 15 (2005), 3670-3674.
- [26] S. Velazquez-Olvera, H. Salgado-Zamora, M. Velazquez-Ponce, E. Campo-Aldrete, A. Reyes-Arellano, C. Perez-Gonzalez, Fluorescent property of 3-hydroxymethyl imidazo[1,2-a]pyridine and pyrimidine derivatives. *Chem. Central J.* 6 (2012) 83-91.
- [27] M. Leopoldo, E. Lacivita, E. Passafiume, M. Contino, N. A. Colabufo, F. Berardi, R. Perrone. 4-[ω-[4-Arylpiperazin-1-yl]alkoxy]phenylimidazo[1,2-a]pyridine derivatives: fluorescent high-affinity dopamine D₃ receptor ligand as potential probe for receptor visualization. *J. Med. Chem.* 50 (2007) 5043-5047.

- [28] S. Martinez Gonzalez, A.I. Hernandez, C. Varela, S. Rodriguez-Aristegui, R.M. Alvarez, Garcia, B. Ana, M. Lorenzo, V. Rivero, J. Oyarzabal, O. Rabal, J.R. Bischoff, M. Albarran, A. Cebria, P. Alfonso, W. Link, J. Fominaya, J. Pastor. Imidazo[1,2-a]pyrazines as novel PI3K inhibitors. *Bioorg. Med. Chem. Letters* 22 (2012) 1874-1878.
- [29] M. Pirtsch, S. Paria, T. Matsuno, H. Isobe, O. Reiser. [Cu(dap)2Cl] As An Efficient Visible-Light-Driven Photoredox Catalyst in Carbon-Carbon Bond-Forming Reactions. *Chemistry - A European Journal* 18 (2012) 7336-7340.
- [30] C. Sablayrolles, P.A. Bonnet, G. Cros, J.P. Chapat, M. Boucard. 8-Alkylaminoimidazo[1,2-a]pyrazine derivatives, their preparation, and their application in therapy. WO 8804298 A1 19880616.
- [31] G. Cristalli, C. Lambertucci, G. Morucci, D. Dal Ben. A_{2A} adenosine receptor and its modulators: an overview on a druggable GPCR and on structure-activity relationship analysis and binding requirements of agonists and antagonists. *Curr. Pharm. Des.* 14 (2008) 1525-1552.
- [32] M. de Lera Ruiz, Y-H, Lim, J. Zeng, Adenosine A_{2A} receptor as a drug discovery target. *J. Med. Chem.* 57 (2014) 3623-3650.
- [33] V.P. Jaakola, M.T. Griffith, M.A. Hanson, V. Cherezov, E.Y. Chien, J.R. Lane, A.P. IJzerman, R.C. Stevens, The 2.6 angstrom crystal structure of a human A_{2A} adenosine receptor bound to an antagonist, *Science* 322 (2008) 1211-1217.
- [34] D. Dal Ben, C. Lambertucci, G. Marucci, R. Volpini, G. Cristalli, Adenosine receptor modeling: what does the A_{2A} crystal structure tell us? *Curr. Top. Med. Chem.* 10 (2010) 993-1018.
- [35] S. Costanzi, A.A Ivanov, I.G. Tikhonova, K.A. Jacobson, Structure and function of G-protein-coupled receptors studied using sequence analysis, molecular modeling, and receptor engineering: adenosine receptors, *Front. Drug Des. Discov.* 3 (2007) 63-69.
- [36] Molecular Operating Environment; C.C.G., Inc., 1255 University St., Suite 1600, Montreal, Quebec, Canada, H3B 3X3.
- [37] Y.C. Kim, X.D. Ji, K.A. Jacobson, Derivatives of the triazoloquinazoline adenosine antagonist (CGS15943) are selective for the human A₃ receptor subtype, *J. Med. Chem.* 39 (1996) 4142-4148.
- [38] J.J. Stewart, MOPAC: a semiempirical molecular orbital program, *J. Comput. Aided Mol. Des.* 4 (1990) 1-105.
- [39] H. Shadnia, J.S. Wright, J.M. Anderson, Interaction force diagrams: new insight into ligand-receptor binding, *J. Comput. Aided Mol. Des.* 23 (2009) 185-194.
- [40] D. Dal Ben, M. Buccioni, C. Lambertucci, G. Marucci, A. Thomas, R. Volpini, G. Cristalli, Molecular modelling study on potent and selective adenosine A₃ receptor agonists, *Bioorg. Med. Chem.* 18 (2010) 7923-7930.

- [41] D. Dal Ben, M. Buccioni, C. Lambertucci, A. Thomas, R. Volpini, Simulation and comparative analysis of binding modes of nucleoside and non-nucleoside agonists at the A_{2B} adenosine receptor, *Silico Pharmacol.* 1 (2013) 24.
- [42] T. Pearson, K. Damian, R.E. Lynas, B.G. Frenguelli, Sustained elevation of extracellular adenosine and activation of A₁ receptors underlie the post-ischaemic inhibition of neuronal function in rat hippocampus *in vitro*. *J Neurochem.* 97 (2006) 1357-1368.
- [43] A.M. Pugliese, C. Traini, S. Cipriani, M. Gianfriddo, T. Mello, M.G. Giovannini, A. Galli, F. Pedata. The adenosine A_{2A} receptor antagonist ZM241385 enhances neuronal survival after oxygen-glucose deprivation in rat CA1 hippocampal slices *Br. J. Pharmacol.* 157 (2009) 818–830.
- [44] A.T R. Williams, S.A. Winfield, J. N. Miller. Relative fluorescence quantum yields using a computer controlled luminescence spectrometer. *Analyst*, 108 (1983) 1067-1071.
- [45] J.R. Lakowicz, *Principles of Fluorescence Spectroscopy*, Kluwer Academic/Plenum Press, New York, 1999, Second Edition.
- [46] F. Mohamadi, N.G.J. Richards, W.C. Guida, R. Liskamp, M. Lipton, C. Caufield, G. Chang, T. Hendrickson, W.C. Still, MacroModel e an integrated software system for modeling organic and bioorganic molecules using molecular mechanics, *J. Comput. Chem.* 11 (1990) 440-467.
- [47] W.D. Cornell, P. Cieplak, C.I. Bayly, I.R. Gould, K.M. Merz, D.M. Ferguson, D.C. Spellmeyer, T. Fox, J.W. Caldwell, P.A. Kollman, A second generation force field for the simulation of proteins, nucleic acids, and organic molecules, *J. Am. Chem. Soc.* 117 (1995) 5179-5197.
- [48] T.A. Halgren, Merck molecular force field. I. Basis, form, scope, parameterization, and performance of MMFF94, *J. Comput. Chem.* 17 (1996) 490-519.
- [49] T.A. Halgren, Merck Molecular Force Field. II. MMFF94 van der Waals and Electrostatic Parameters for Intermolecular Interactions, *J. Comput. Chem.* 17 (1996) 520-552.
- [50] T.A. Halgren, Merck molecular force field. III. Molecular geometries and vibrational frequencies for MMFF94, *J. Comput. Chem.* 17 (1996) 553-586.
- [51] T.A. Halgren, Merck molecular force field. IV. Conformational energies and geometries for MMFF94, *J. Comput. Chem.* 17 (1996) 587-615.
- [52] T.A. Halgren, R. Nachbar, Merck molecular force field. V. Extension of MMFF94 using experimental data, additional computational data, and empirical rules, *J. Comput. Chem.* 17 (1996) 616-641.
- [53] T.A. Halgren, MMFF VI. MMFF94s option for energy minimization studies, *J. Comput. Chem.* 20 (1999) 720-729.

- [54] T.A. Halgren, MMFF VII. Characterization of MMFF94, MMFF94s, and other widely available force Fields for conformational energies and for intermolecular-interaction energies and geometries, *J. Comput. Chem.* 20 (1999) 730-748.
- [55] D. Dal Ben, M. Buccioni, C. Lambertucci, S. Kachler, N. Falgner, G. Marucci, A. Thomas, G. Cristalli, R. Volpini, K.-N. Klotz, Different efficacy of adenosine and NECA derivatives at the human A₃ adenosine receptor: insight into the receptor activation switch, *Biochem. Pharmacol.* 87 (2014) 321-331.
- [56] F. Vincenzi, M. Targa, R. Romagnoli, S. Merighi, S. Gessi, P.G. Baraldi, P.A. Borea, K. Varani, Tr469, a Potent A₁ Adenosine Receptor Allosteric Modulator, Exhibits Anti-nociceptive Properties in Acute and Neuropathic Pain Models in Mice. *Neuropharmacology* 81 (2014) 6-14.
- [57] K. Varani, A. Massara, F. Vincenzi, A. Tosi, M. Padovan, F. Trotta, P.A. Borea, Normalization of A_{2A} and A₃ Adenosine Receptor Up-regulation in Rheumatoid Arthritis Patients by Treatment with Anti-tumor Necrosis Factor Alpha but not Methotrexate. *Arthritis Rheum.* 60 (2009) 2880-2891.
- [58] K. Varani, S. Merighi, S. Gessi, K.N. Klotz, E. Leung, P.G. Baraldi, B. Cacciari, R. Romagnoli, G. Spalluto, P.A. Borea, [3H]-MRE 3008-F20: a novel antagonist radioligand for the pharmacological and biochemical characterization of human A₃ adenosine receptors, *Mol. Pharmacol.* 57 (2000) 968-975.
- [59] K. Varani, S. Gessi, S. Merighi, F. Vincenzi, E. Cattabriga, A. Benini, K.-N. Klotz, P.G. Baraldi, M.-A. Tabrizi, S. Mac Lennan, E. Leung, P.A. Borea, Pharmacological characterization of novel adenosine ligands in recombinant and native human A_{2B} receptors, *Biochem. Pharmacol.* 70 (2005) 1601-1612.
- [60] A.M. Pugliese, E. Coppi, G. Spalluto, R. Corradetti, F. Pedata, A₃ adenosine receptor antagonists delay irreversible synaptic failure caused by oxygen and glucose deprivation in the rat CA1 hippocampus in vitro. *Br. J. Pharmacol.* 147 (2006) 524–532.
- [61] W.W. Anderson, G.L. Collingridge, The LTP Program: a data acquisition program for on-line analysis of long-term potentiation and other synaptic events. *J. Neurosci. Methods* 108 (2001) 71-83.
- [62] E. Farkas, R. Pratt, F. Sengpiel, T.P. Obrenovitch, Direct, live imaging of cortical spreading depression and anoxic depolarization using a fluorescent, voltage-sensitive dye. *J. Cereb. Blood Flow Metab.* 28 (2008) 251–262.
- [63] F. Pedata, S. Latini, A.M. Pugliese, G. Pepeu, Investigations into the adenosine outflow from hippocampal slices evoked by ischemialike conditions. *J. Neurochem.* 61 (1993) 284–289.

Figure Captions.

Figure 1. Previously reported pyrazolo[4,3-*d*]pyrimidine derivatives (**PP**).

Figure 2. Currently reported imidazo[1,2-*a*]pyrazine derivatives as AR antagonists.

Figure 3. Docking conformations of the 2,6,8-substituted imidazopyrazine derivatives. (A) The binding mode of compound **22** at 3EML-based hA₃AR model is shown as an example. (B) Schematic view of ligand-receptor interaction for the same compound.

Figure 4. Docking conformations of the 2,8-substituted imidazopyrazine derivatives. (A) The binding mode of compound **6** (green) at 3EML-based hA₃AR model is shown as an example. The docking mode of compound **22** (light pink) is shown for comparison. (B) Schematic view of ligand-receptor interaction for the same compound.

Figure 5. Docking conformation of compounds **21** (A) and **22** (B). Molecular surfaces of both the ligand (dark) and the cavity (light) are represented. Comparison highlights the higher volume complementarity between the cavity and compound **22** with respect to that of compound **21**. (C) Detailed view of the interaction of the 8-substituent of compound **22** with the nearby residues. (D) Ligand–receptor interaction energies (per-residue values) calculated with IF-E 6.0 script. Data of interaction between the receptor and the aromatic group within the 8-substituent are represented. See text for details.

Figure 6. Compound **29** significantly delayed the appearance of AD induced by 30-min OGD in rat hippocampal slices. The graph shows the d.c. shift traces during 30-min OGD in untreated slices (OGD, *n* = 5) (A) or in slices treated with compound **29** (200 nM, *n* = 8) (B). (a) Each column represents the mean (\pm SEM) of AD latency recorded in hippocampal slices during 30-min OGD in the absence (OGD) or in the presence of 200 nM compound **29** (OGD + compound **29**, *n*=8). AD was measured from the beginning of OGD insult. Note that compound **29** significantly delayed AD development. **P* < 0.05, unpaired two-tailed Student's *t*-test in comparison to untreated OGD slices. (b) Each column represents the mean (\pm SEM) of AD amplitude, recorded in hippocampal slices during 30-min OGD, in the absence or in the presence of 200 nM compound **29** (OGD + compound **29**, *n*=8). The number (*n*) of slices tested is reported inside columns. (C) Graph shows the time course of 7-min OGD effects on fEPSP amplitude in an untreated OGD slice and in compound **29**-treated OGD slice. Amplitude of fEPSP is expressed as percent of pre-ischemic baseline. Note that, after reperfusion in normal oxygenated aCSF, a significant recovery of fEPSP was found only in compound **29**-treated OGD slices.

Scheme 1. Reagents and conditions: a) BrCH₂COR₂, 100°C; b) NH₃ (gas), absolute ethanol, 120°C, autoclave; c) H₂, Pd/C, ethanol; d) RCOCl, anhydrous tetrahydrofuran, pyridine, reflux, or RCOOH, N-(3-dimethylammino-propyl)-N'-ethylcarbodiimide·HCl, 1-hydroxybenzotriazole hydrate, anhydrous dimethylformamide, r.t.; e) PhNCO, anhydrous dichloromethane, r.t.

Scheme 2. Reagents and conditions: a) C₆H₅B(OH)₂, tetrakis, Na₂CO₃, 1,2-dimethoxyethane/water 3:1, 85°C; b) RCOCl, pyridine, reflux.

Scheme 3. Reagents and conditions: a) Commercially available R₆B(OH)₂ or **42** (R₆ = 3-(C₆H₅CH₂CONH)C₆H₄), tetrakis, Na₂CO₃, dimethoxyethane/water 3:1, 85°C.

Table 1. Binding affinity (K_i) at hA_1 , hA_{2A} and hA_3 ARs and potencies (IC_{50}) at hA_{2B} .

Table 2. Binding affinity (K_i) at hA_1 , hA_{2A} and hA_3 ARs and potencies (IC_{50}) at hA_{2B} .

Table 3. Antagonistic potencies at hA_3 and binding affinity at rA_3 AR of some selected derivatives.

Table 4. Fluorescence properties of some imidazopyrazine derivatives^a.

Supplementary data

Imidazo[1,2-*a*]pyrazin-8-amine core for the design of new adenosine receptor antagonists: structural exploration to target the A₃ and A_{2A} subtypes.

Daniela Poli,^a Matteo Falsini,^a Flavia Varano,^a Marco Betti,^a Katia Varani,^b Fabrizio Vincenzi,^b Anna Maria Pugliese,^c Felicita Pedata,^c Diego Dal Ben,^d Ajiroghene Thomas,^d Ilaria Palchetti,^{e,f} Francesca Bettazzi,^e Daniela Catarzi,^{a*} Vittoria Colotta^a

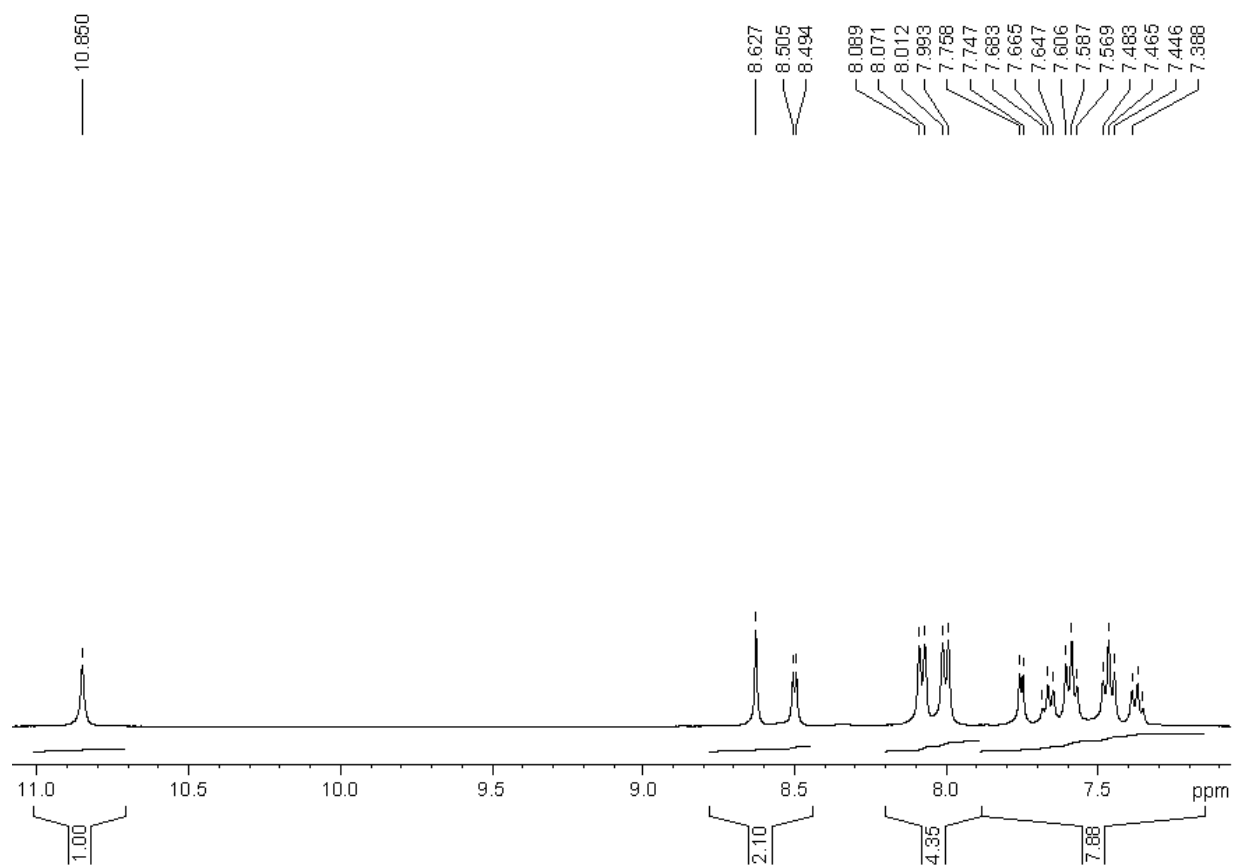
^aDipartimento di Neuroscienze, Psicologia, Area del Farmaco e Salute del Bambino, Sez. Farmaceutica e Nutraceutica, Università degli Studi di Firenze, Via Ugo Schiff 6, 50019 Sesto Fiorentino (FI) Italy; ^bDipartimento di Scienze Mediche, Sez. Farmacologia, Università degli Studi di Ferrara, Via Fossato di Mortara, 17-19, 4412 Ferrara, Italy; ^cDipartimento di Neuroscienze, Psicologia, Area del Farmaco e Salute del Bambino, Sez. Farmacologia e Tossicologia, Università degli Studi di Firenze, Viale Pieraccini, 6, 50139 Firenze, Italy; ^dScuola di Scienze del Farmaco e dei Prodotti della Salute, Università degli Studi di Camerino, Via S. Agostino 1, 62032 Camerino (MC), Italy; ^eDipartimento di Chimica "Ugo Schiff", Università degli Studi di Firenze, Via della Lastruccia 3-13, 50019 Sesto Fiorentino (FI) Italy, ^fIstituto di Biochimica delle Proteine-CNR, Via P. Castellino 111, 80131 Napoli, Italy.

Contents:

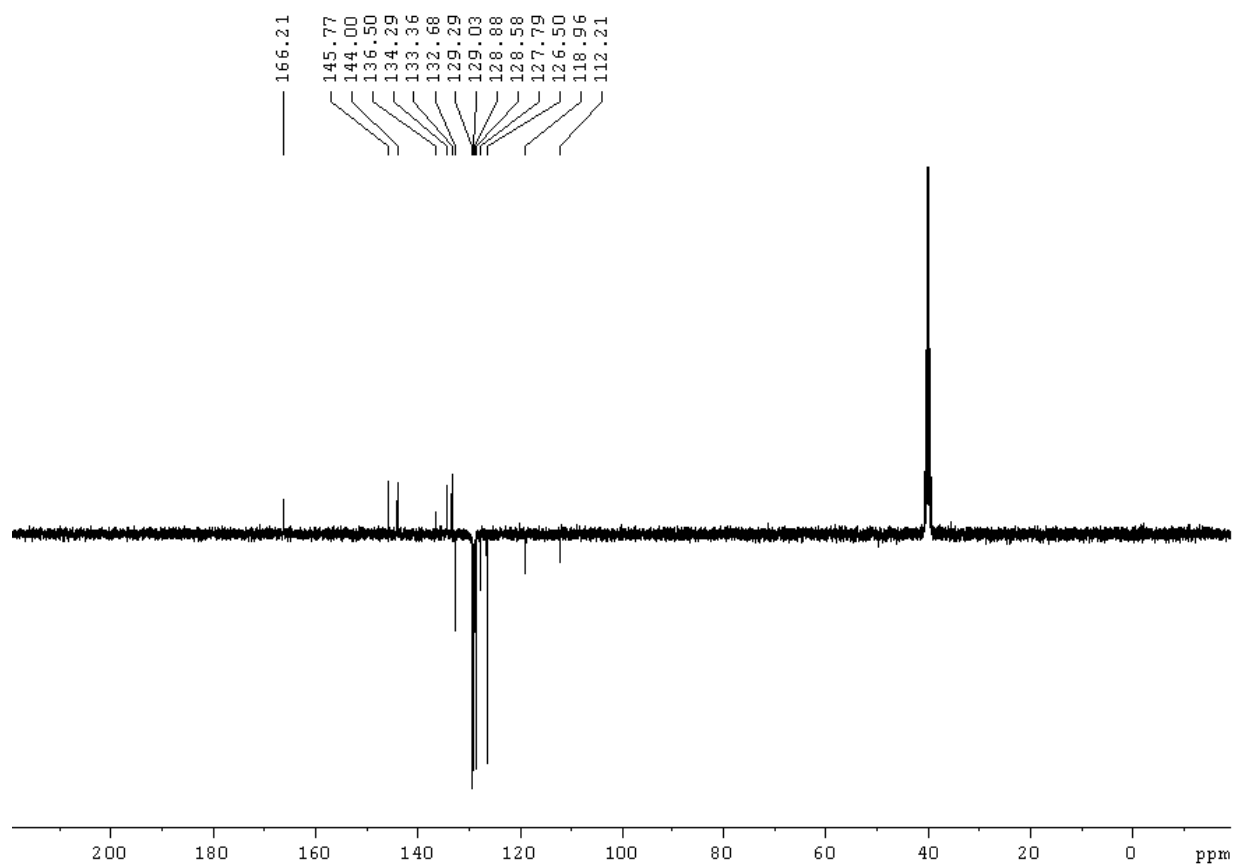
¹H NMR and ¹³C APT NMR spectra of some selected derivatives (.....).

The ¹³C APT (Attached Proton Test) experiment distinguishes between C-H multiplicities. CH and CH₃ vectors have opposite phases compared to C and CH₂. Therefore, the phase of CH and CH₃ peaks is 180° different from C (including the solvent DMSO) and CH₂ peaks.

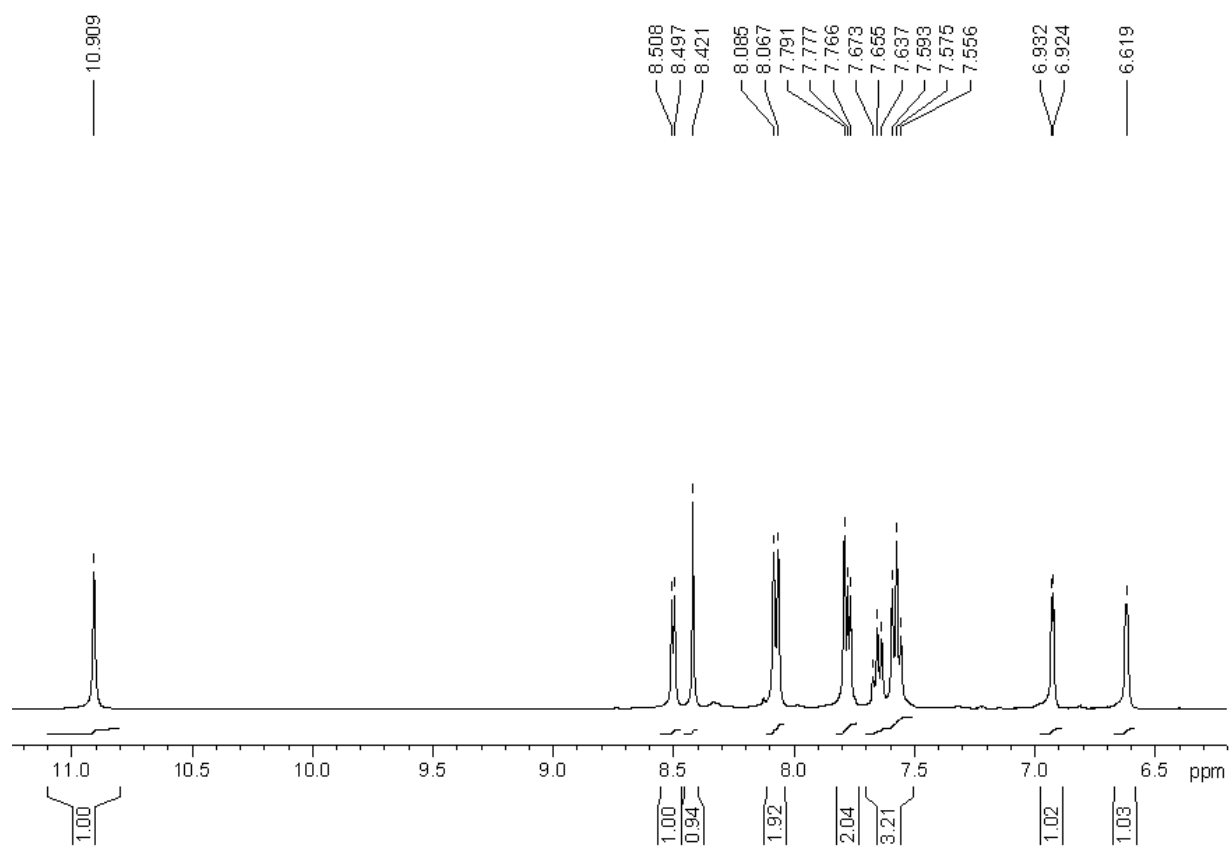
^1H NMR spectrum (400 MHz, DMSO-d_6) of compound **4**.



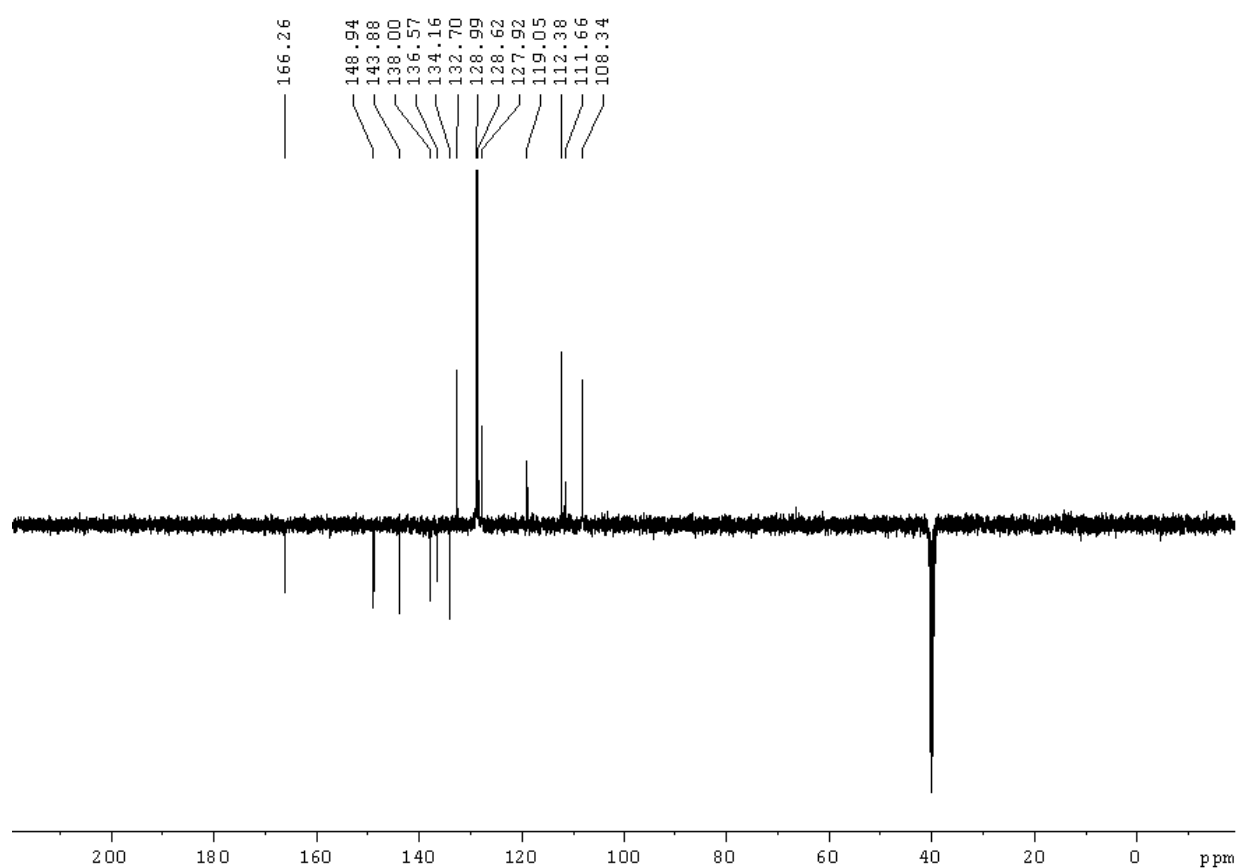
^{13}C APT NMR spectrum (100 MHz, DMSO-d_6) of compound **4**.



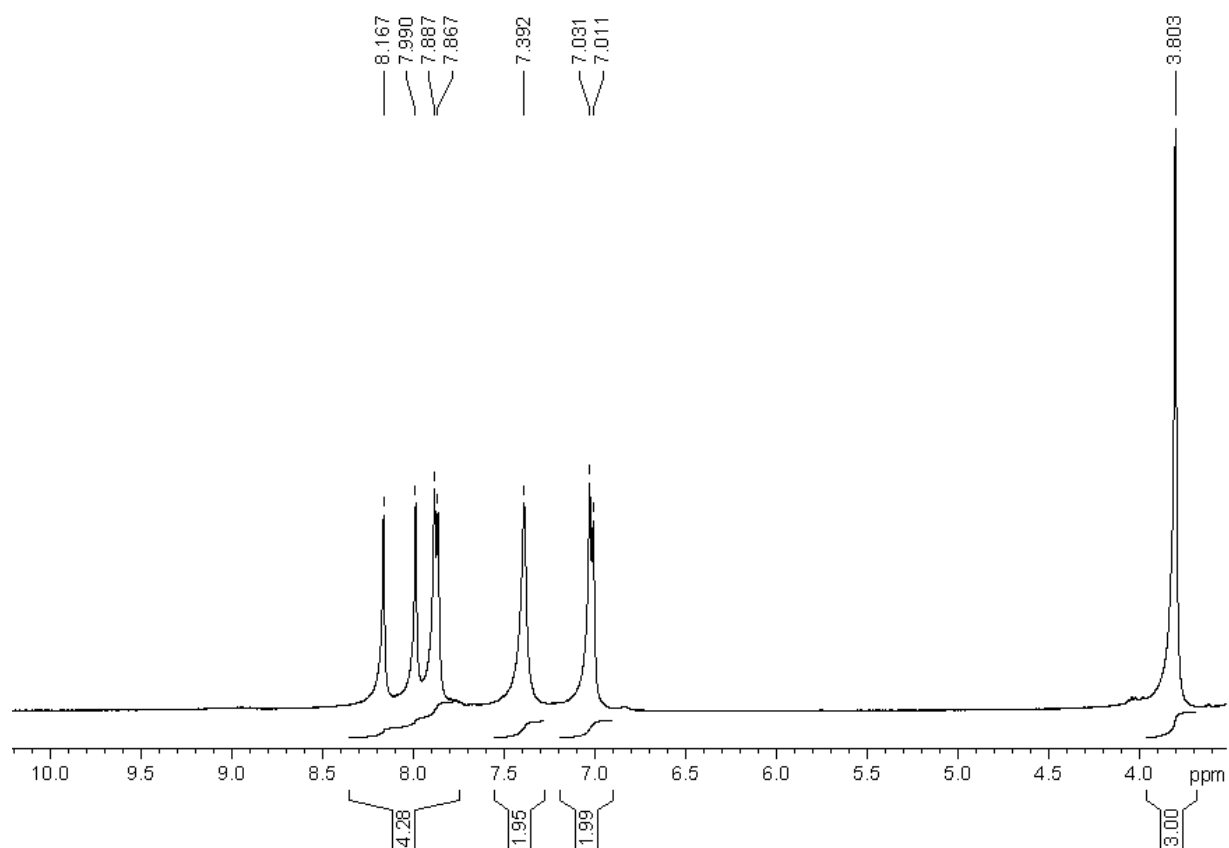
^{13}C NMR spectrum (400 MHz, DMSO- d_6) of compound **13**.



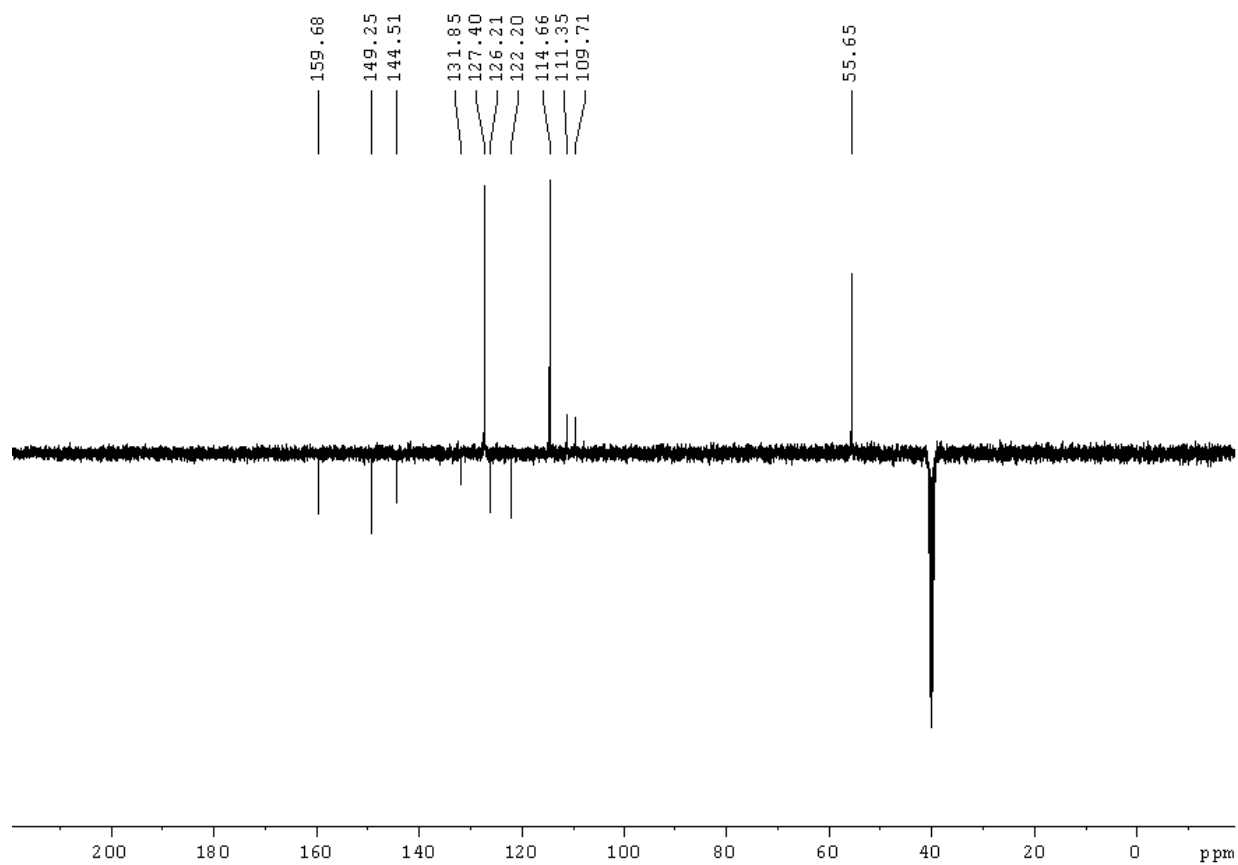
^{13}C APT NMR spectrum (100 MHz, DMSO- d_6) of compound **13**.



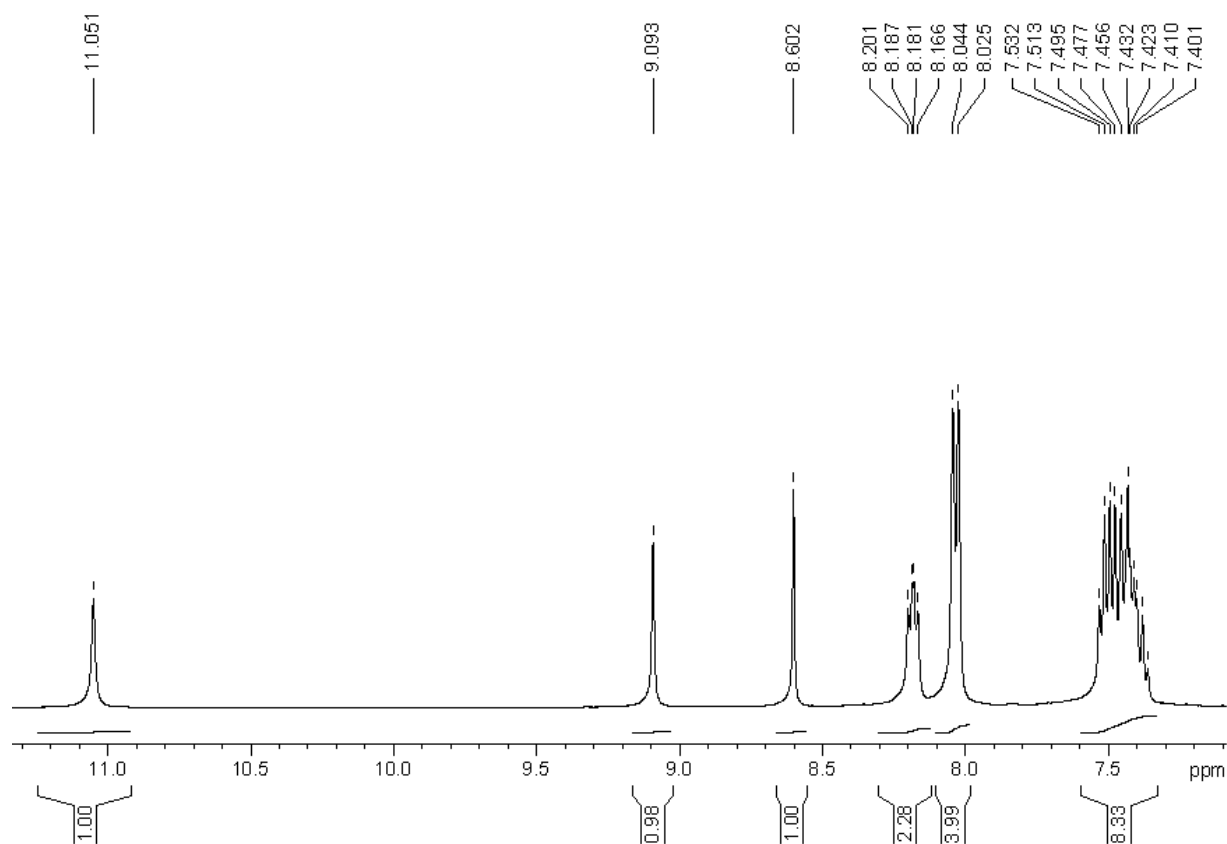
^1H NMR spectrum (400 MHz, DMSO- d_6) of compound **16**.



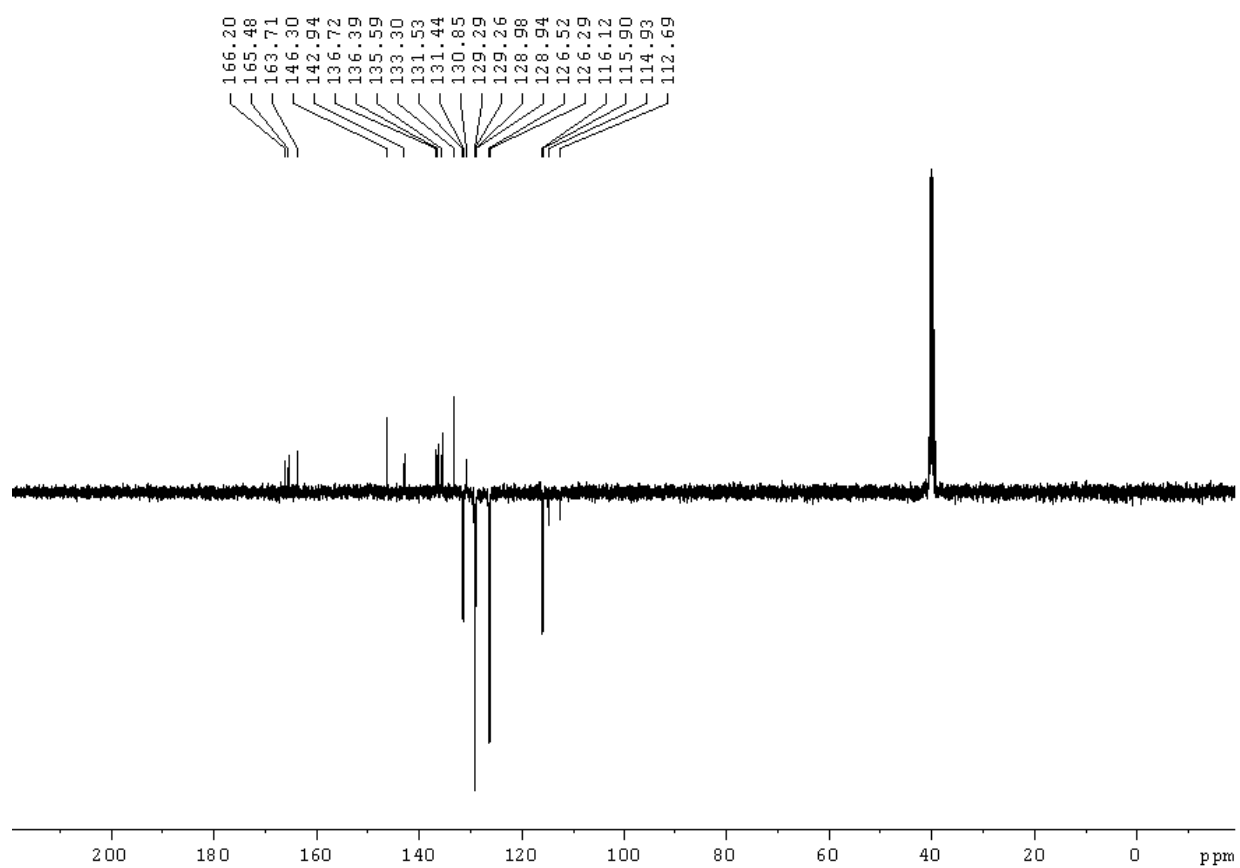
^{13}C APT NMR spectrum (100 MHz, DMSO-d_6) of compound **16**.



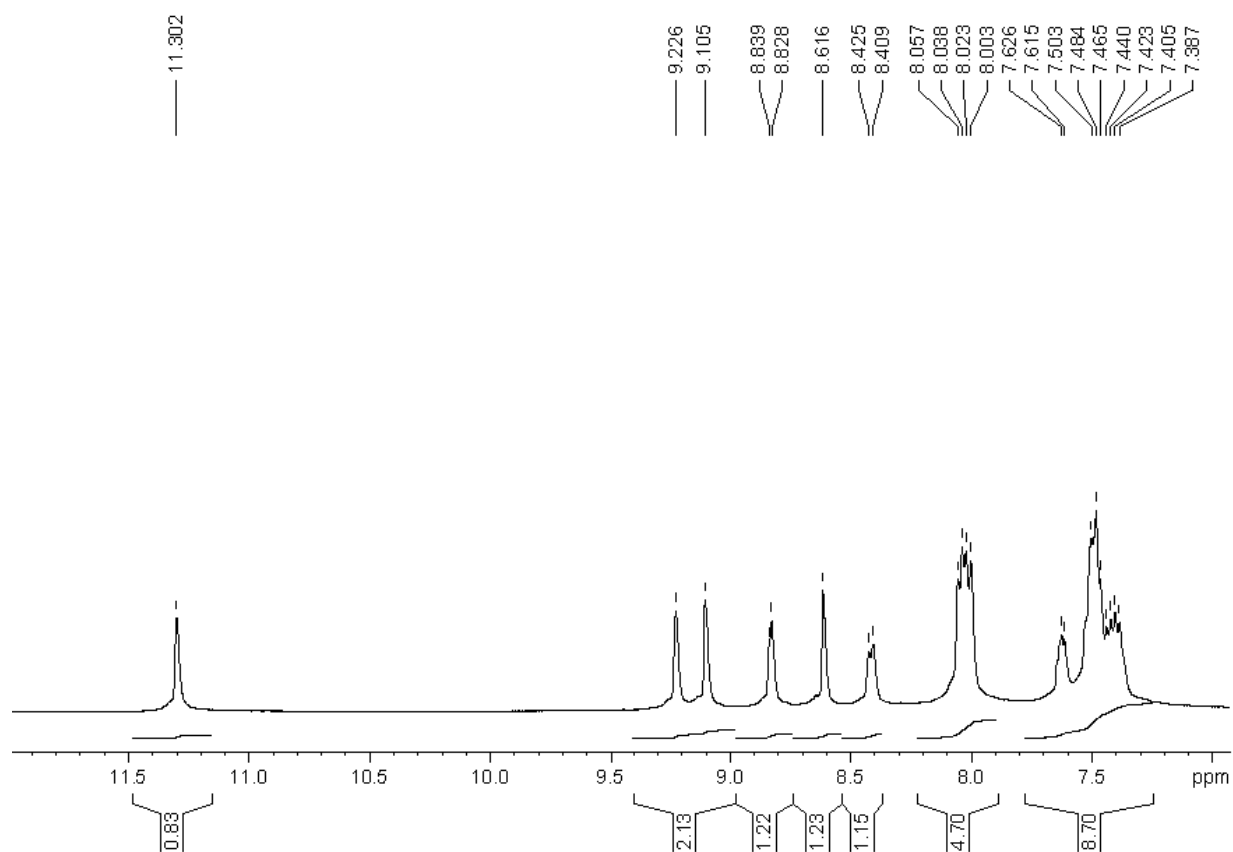
^1H NMR spectrum (400 MHz, DMSO-d_6) of compound **25**.



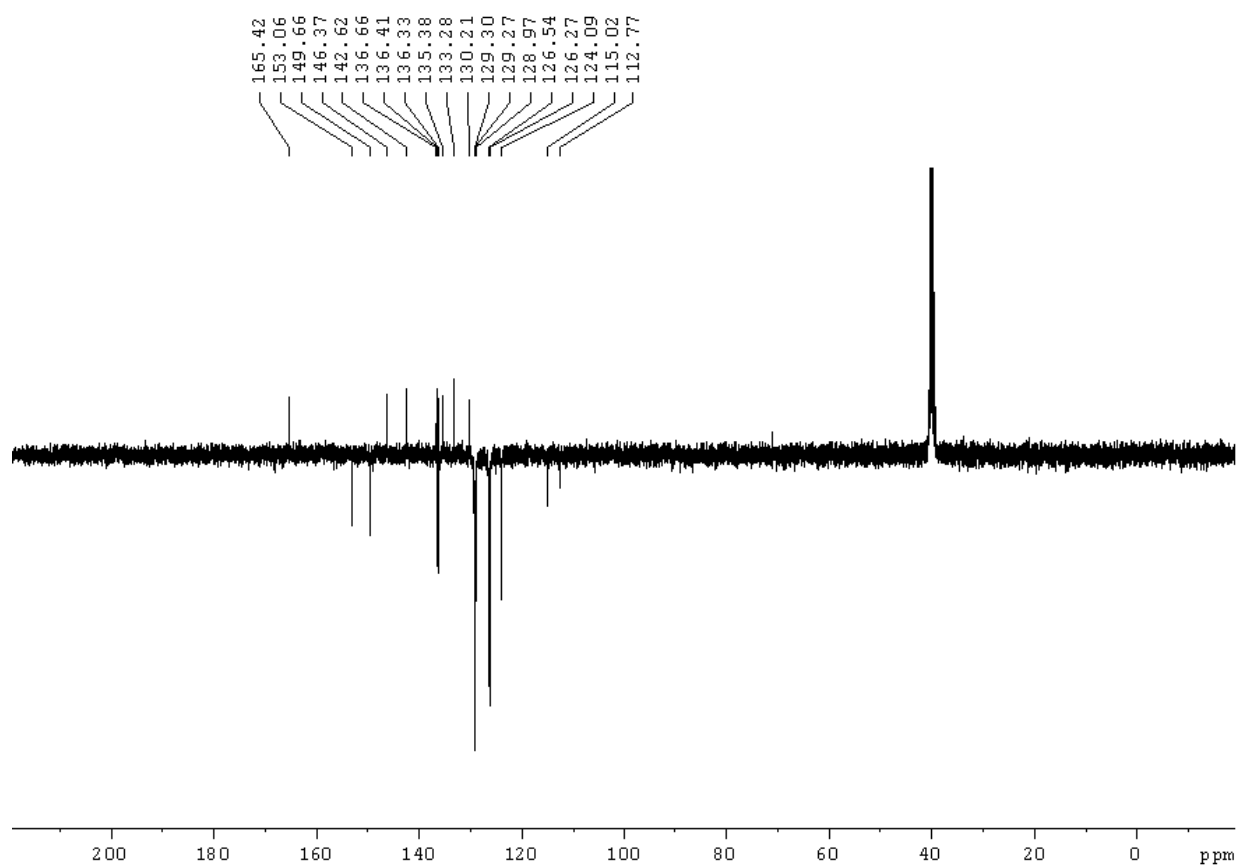
^{13}C APT NMR spectrum (100 MHz, DMSO-d_6) of compound **25**.



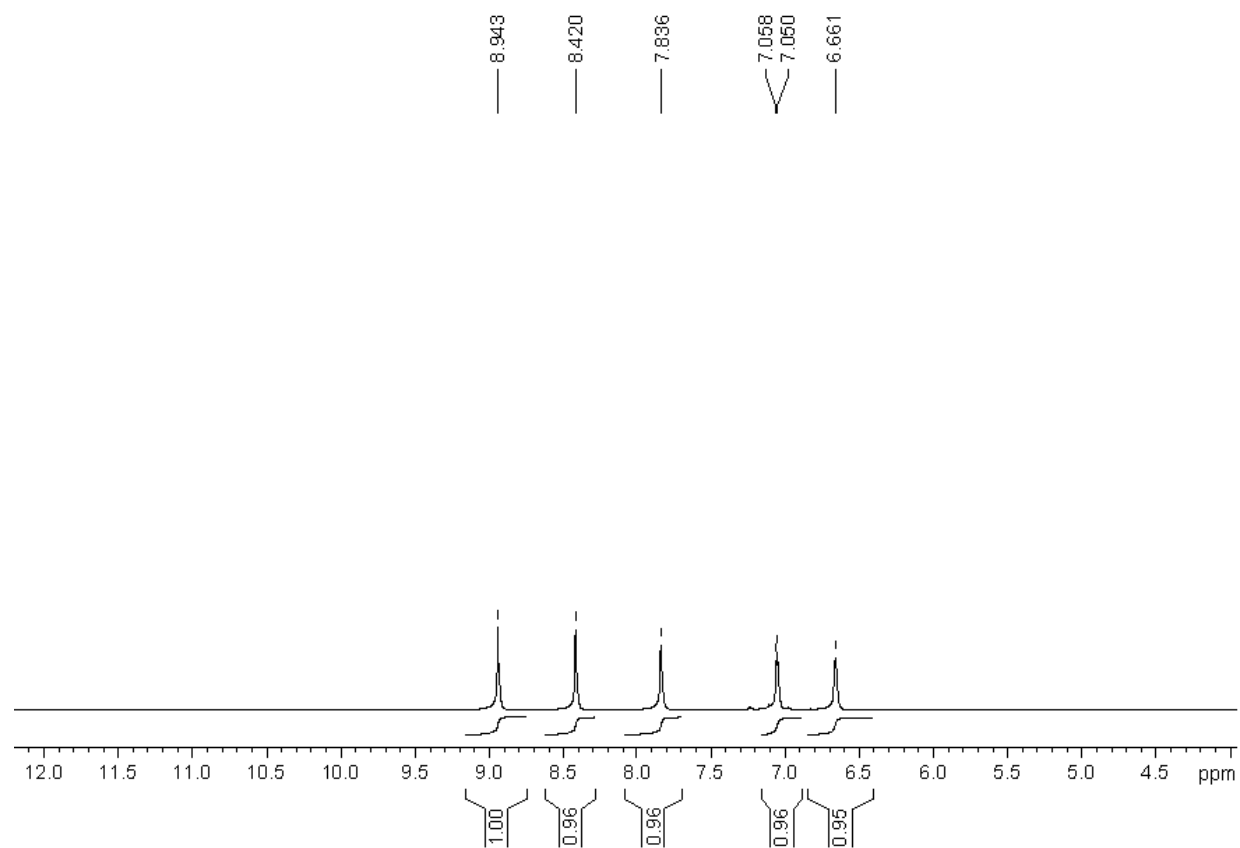
^{13}C NMR spectrum (400 MHz, DMSO- d_6) of compound **29**.



^{13}C APT NMR spectrum (100 MHz, DMSO-d_6) of compound **29**.



^1H NMR spectrum (400 MHz, DMSO-d_6) of compound **41**.



^{13}C APT NMR spectrum (100 MHz, DMSO-d_6) of compound **41**.

